Molecular Therapy
Oncolytics
Original Article

The PABPC5/HCG15/ZNF331 Feedback Loop Regulates Vasculogenic Mimicry of Glioma via STAU1-Mediated mRNA Decay

Fangkun Jing,[1,2,3] Xuelei Ruan,[4,5,6] Xiaobai Liu,[1,2,3] Chunqing Yang,[1,2,3] Di Wang,[1,2,3] Jian Zheng,[1,2,3] Yixue Xue,[4,5,6] Shuyuan Shen,[4,5,6] Lianqi Shao,[4,5,6] Yang Yang,[1,2,3] Ping Wang,[4,5,6] Jun Ma,[4,5,6] and Yunhui Liu[1,2,3]

[1]Department of Neurosurgery, Shengjing Hospital of China Medical University, Shenyang 110004, China; [2]Liaoning Clinical Medical Research Center in Nervous System Disease, Shenyang 110004, China; [3]Key Laboratory of Neuro-oncology in Liaoning Province, Shenyang 110004, China; [4]Department of Neurobiology, School of Life Sciences, China Medical University, Shenyang 110122, China; [5]Key Laboratory of Cell Biology, Ministry of Public Health of China, China Medical University, Shenyang 110122, China; [6]Key Laboratory of Medical Cell Biology, Ministry of Education of China, China Medical University, Shenyang 110122, China

Glioma is the most common primary malignancy in the brain, and vasculogenic mimicry (VM) is one of the blood supply methods. Here we investigated the possibility that lncRNAs regulate the stability of transcription factors through the SMD pathway, which affects proliferation, migration, invasion, and the ability to form VMs in glioma. Expression of *PABPC5*, *HCG15*, and *ZNF331* was detected by real-time qPCR or western blot in glioma. Cell Counting Kit-8, Transwell assays, and *in vitro* VM tube formation were used to investigate *PABPC5*, *HCG15*, and *ZNF331* function in cell proliferation, migration, invasion, and VM, respectively. ChIP assays were used to ascertain the interaction between*ZNF331* and *LAMC2* or *PABPC5*. *PABPC5* and *HCG15* were highly expressed in glioma cells. *ZNF331* was lowly expressed. *PABPC5* bound *HCG15* to increase its stability. Knockdown *HCG15* reduced the degradation of ZNF331 mRNA by the SMD pathway. *ZNF331* inhibited transcription through binding to the promoter region of *LAMC2* and *PABPC5* and inhibited the ability to form VMs in glioma cells. The *PABPC5/HCG15/ZNF331* feedback loop plays an important role in regulating VM formation in glioma and provides new targets for glioma treatment.

INTRODUCTION

Glioma is the most common and malignant central nervous system tumor in humans, accounting for 60% of central tumors, with a mortality rate of more than 98%. Currently, glioma treatment methods mainly include surgery, radiation therapy, and chemotherapy,[1,2] Although the symptoms can be improved by active treatment, treatment effects are still not satisfactory, the recurrence rate is high, the 2-year survival rate is only 15% −26%, and the average median survival time is only 12–18 months.[3] Gliomas are primary intracranial malignancies with the highest degree of vascularization and characterized by micro-angiogenesis and angiogenesis.[4] Currently, anti-vascular therapies include tyrosine kinase inhibitors and recombinant humanized monoclonal antibodies. Various cancer treatments have been extensively studied,[5] and similarly targeted anti-angiogenic drugs can be effective for glioma treatment.[6] Several related studies have concluded that vasculogenic mimics help to generate anti-angiogenic therapeutic resistance, resulting in poor anti-angiogenic treatment effects.[7,8] Therefore, research regarding the vasculogenic mimic mechanism of glioma cells can provide new treatment strategies for glioma chemotherapy and improve treatment effects.

Maniotis et al.[9] proposed the concept of vasculogenic mimicry (VM) when they studied melanoma in 1999. Some studies have shown that tumor cells directly generate vascular channels and are independent on endothelial cells. Vascular channels are blood vessel-like pipe structures formed by malignant tumor cells in a state of hypoxia to meet the needs of their own blood supply to develop their own growth;[10] this provided a new perspective regarding tumor cell plasticity.[11] Tumor samples are used for immunohistochemistry (IHC) to identify VM; tumor VM periodic acid Schiff (PAS) staining is positive, and CD31 or CD34 staining is negative, indicating the presence of matrix-associated vascular channels.[12] In recent years, research regarding anti-VM has become a new direction for glioma treatment. Therefore, the study of tumor vascular mimicry-related genes and signal transduction pathways is of great significance.[13] Studies have reported that glioma VM is positively correlated with malignancy and promotes glioma migration, invasion, and metastasis.[14,15]

RNA binding proteins (RBPs) accompany the formation and metabolism of RNA, regulate the stability of RNA, and participate in mediating RNA transport and translation.[16] RBPs regulate the occurrence and development of tumors, including continuous cell proliferation, reducing apoptosis, evading surveillance by the immune system, inducing angiogenesis, and activating metastasis.[17] *PABPC5* (poly(A)

Received 18 February 2020; accepted 25 March 2020;
https://doi.org/10.1016/j.omto.2020.03.017.

Correspondence: Yunhui Liu, Shengjing Hospital of China Medical University, Shenyang 110004, China.
E-mail: liuyh_cmuns@163.com; 174872115@qq.com; xueyixue888@163.com

binding protein cytoplasmic 5) is a member of the cytosolic poly(A) binding protein family, binds to the protein at the 3′ end of the poly(A) tail of most eukaryotic mRNAs, and is located on chromosome Xq21.3/Yp11.2.[18] Studies have suggested that *PABPC5* is involved in metabolism of DNA and RNA in mitochondria. The *PABPC5* gene is composed of at least two exons and one intron and an uninterrupted ORF (open reading frame).[19] Studies have found that *PABPC5* is located on translocation breakpoint *DX214*, associated with premature ovarian failure in ovarian disease, and high expression of *PABPC5* is closely related to the poor prognosis of ovarian cancer patients.[20] At present, there are no reports of glioma research.

Imbalance of non-coding RNA (ncRNA) is related to the progression of various tumors and plays an important regulatory role in tumorigenesis and development,[21] including long ncRNA (lncRNA; >200 nt) and microRNA (miRNA; ~22 nt)).[22] lncRNA is involved in various cellular processes, such as proliferation, migration, invasion, and apoptosis.[22] A large amount of evidence proves that lncRNA plays a key role in the progression of gliomas and also has important significance for the diagnosis and treatment of gliomas.[23] *HCG15* (Human leukocyte antigen complex group 15) is located on chromosome 6p21.[24] At present, *HCG15* has not been reported in glioma and VM.

STAU (Staufen) is a key mRNA transport and localization factor in *Drosophila*. Combination of the *Stau* paralog *Stau1* in mammals with the 3′ UTR region of intermolecular and intramolecular double-stranded structures triggers degradation of target mRNA;[25] this degradation process is called Staufen-mediated mRNA decay (SMD). SMD is a *STAU1* mediated mRNA degradation pathway, which *STAU1* combines with *STAU1* binding site (SBS) formed when the Alu element of lncRNAs recognizes and pairs with the Alu element of target mRNA 3'UTR during translation, and then recruits the ATP-dependent RNA helicase up-frameshift 1 (*UPF1*) to bind and promote the degradation of target mRNA. *UPF1* can detect and degrade mRNA transcripts containing premature stop codons (PTCs), specifically accelerating the target degradation of gene mRNA.[26] Studies have reported that approximately 1% of human mRNA is regulated by *STAU1*, so SMD is an important post-transcriptional regulatory pathway.[27] The role of SMD in glioma needs further investigation.

In cancer research, LINC00993 regulates the development of breast cancer by inhibiting *CDKN2A* transcription.[28] *ZNF331* (zinc-finger protein 331) is located on chromosome 19q13.42, which encodes a zinc-finger protein containing the KRAB (Kruppel-related box) domain found in transcriptional repressors. Studies have reported that *ZNF331* methylates in the promoter region of human gastric cancer cells, which inactivates them and increases the growth and invasion capabilities of gastric cancer cells.[29] Low expression of *ZNF331* indicates a poor prognosis in colorectal cancer patients.[30] At present, no research of *ZNF331* regulating VM of gliomas has been reported.

LAMC2 (laminin subunit gamma 2) is a family of extracellular matrix glycoproteins. It is the main non-collagen component of the basement membrane and is involved in regulating a variety of biological processes, including cell adhesion, differentiation, migration, signaling, neurite growth, and metastasis.[31] *LAMC2* promotes the migration and invasion of lung cancer cells through the Protein kinase B (PKB or AKT) signaling pathway.[32] Studies have reported that *LAMC2* is highly expressed in U87 and U251 glioma cells.[33,34] *LAMC2* plays a key role in formation of glioma vascular mimicry through the AKT and ERK(extracellular regulated protein kinases) signaling pathways, and it increase the malignancy degree of glioma.[34] The tumor blood supply channel is formed by deformation of the extracellular matrix, so *LAMC2* is a landmark protein for VM. *ZNF331* has not been found to regulate the transcription of *LAMC2* and, thus, to regulate VM in glioma.

In this study, we investigated the expression and function of *PABPC5*, *HCG15*, and *ZNF331* in glioma tissue and glioma cell lines and studied the role of *PABPC5*, *HCG15*, and *ZNF331* in regulating glioma VM. These results will provide new molecular mechanisms for glioma development and provide new insights into glioma treatment.

RESULT

PABPC5 and *HCG15* Were Highly Expressed in Glioma Tissues and Cells, and Knockdown of *PABPC5* and *HCG15* Inhibited VM Formation

Western blot was used to detect *PABPC5* expression in glioma tissues (12 normal brain tissues, 12 low-grade glioma tissues [World Health Organization [WHO] I–II], and 12 high-grade glioma tissues [WHO III–IV]) and glioma cells (U87 and U251). As shown in Figures 1A and 1B, compared with the normal brain tissue group, expression of *PABPC5* was significantly increased in low-grade glioma tissue and high-grade glioma tissue ($p < 0.01$); the expression of *PABPC5* was significantly higher than in low-grade glioma tissues ($p < 0.05$). In U87 and U251 glioma cells, the expression level of *PABPC5* was significantly higher than in the normal human astrocyte (NHA) group ($p < 0.05$). To further explore the function of *PABPC5* in gliomas and construct knockdown *PABPC5* cells, we applied two knockdown plasmids to transfect glioma cells and tested the transfection efficiency. We selected the higher knockdown efficiency. The #2 plasmid was subjected to subsequent experiments ($p < 0.01$) (Figure S1B). The results showed that knockdown of *PABPC5* affected proliferation, migration, invasion, and VM in glioma cells. As shown in Figures 1C–1E, compared with the *PABPC5 (–)-NC* group, the proliferation, migration, invasion, and VM formation ability of cells in the *PABPC5 (–)* group were significantly reduced ($p < 0.01$). The expression of *LAMC2* in the control group was not significantly different from that of the *PABPC5 (–)-NC* group; compared with the *PABPC5 (–)-NC* group, the expression of *LAMC2* in the *PABPC5 (–)* group was significantly reduced ($p < 0.01$ and $p < 0.05$) (Figure 1F).

HCG15 expression was detected in glioma tissues (12 normal brain tissues, 12 low-grade glioma tissues [WHO I–II], and 12 high-grade glioma tissues [WHO III–IV]) and in glioma cells (U87 and U251)

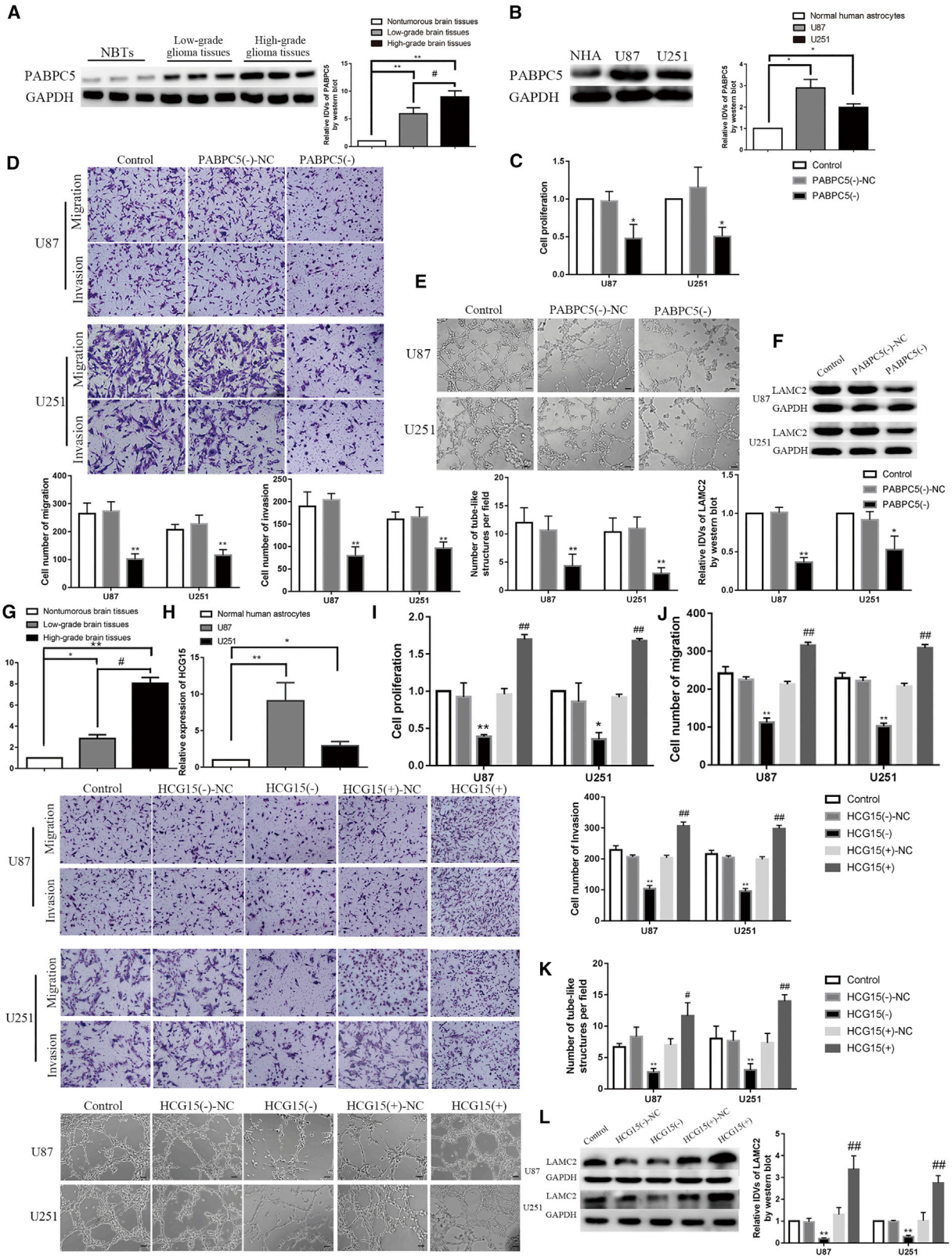

(legend on next page)

by real-time qPCR technology. The results are shown in Figures 1G and 1H. Compared with the normal brain tissue group, the expression of *HCG15* in low-grade glioma tissue ($p < 0.05$) and high-grade glioma tissue ($p < 0.01$) was significantly higher than in normal brain tissue. The expression of *HCG15* in high-grade glioma tissue was significantly higher than in low-grade glioma tissue ($p < 0.05$). The expression of *HCG15* in U87 and U251 glioma cells was significantly higher than in the NHA group ($p < 0.01$ and $p < 0.05$). To further analyze the effects of *HCG15* knockdown and overexpression on the biological behavior of gliomas, we constructed knockdown and overexpression *HCG15* cell lines. In knockdown *HCG15* cell lines, we transfected with two knockdown plasmids and tested transfection efficiency. We selected #2 with the higher knockdown efficiency for subsequent experiments ($p < 0.01$) (Figure S1C). We tested transfection efficiency for glioma cells transfected with overexpression of *HCG15*; its expression increased about 3 times ($p < 0.01$) (Figure S1D). We investigated the effects on proliferation, migration, invasion, and VM ability in glioma cells. The results are shown in Figures 1I–1L. Compared with the control group, there was no statistical difference between the *HCG15 (–)-NC* and *HCG15 (+)-NC* groups; compared with the *HCG15 (–)-NC* group, the *HCG15 (–)* group had significantly reduced proliferation, migration, invasion, and VM ability of glioma cells ($p < 0.01$, $p < 0.05$) and significantly reduced expression levels of the vascular mimicry-related molecule *LAMC2* in glioma cells ($p < 0.01$). Compared with the *HCG15 (+)-NC* group, the *HCG15 (+)* group significantly increased the proliferation, migration, invasion, and VM ability in glioma cells ($p < 0.01$) and increased expression levels of the vascular mimicry-related molecule *LAMC2* in glioma cells ($p < 0.01$).

PABPC5 Promoted VM Formation in Glioma Cells by Increasing the Stability of *HCG15*

Next, the effect of *PABPC5* knockdown on *HCG15* was detected. The results are shown in Figure 2A. Compared with the control group, the expression of *HCG15* was not significantly different in the *PABPC5 (–)-NC* group; compared with the *PABPC5 (–)-NC* group, the expression level of *HCG15*was significantly reduced in *PABPC5 (–)* group ($p < 0.01$). To study the relationship between *PABPC5* and *HCG15*, RNA immunoprecipitation (IP) experiments were used to detect whether there was a direct binding effect between *PABPC5* and *HCG15*. As shown in Figure 2B, in the anti-*PABPC5* group, *HCG15* enrichment was significantly higher than in the anti-immunoglobulin G (IgG) group ($p < 0.01$ and $p < 0.05$). Furthermore, the effect of *PABPC5* knockdown on *HCG15* nascent was detected; there was no statistical difference between the control group and the *PABPC5 (–)-NC* group, and there was no difference between the *PABPC5 (–)-NC* group and the *PABPC5 (–)* group (Figure 2C). Half-life experiments (Figure 2D) confirmed that there was no significant statistical difference between the control group and the *PABPC5 (–)-NC* group; compared with the *PABPC5 (–)-NC* group, the half-life of *HCG15* was significantly reduced in the *PABPC5 (–)* group ($p < 0.01$ and $p < 0.05$). Knockdown of *PABPC5* combined with knockdown and overexpression of *HCG15* were performed in a glioma cell line. Furthermore, the effects of *PABPC5* knockdown cotransfection with overexpression of *HCG15* on proliferation, migration, invasion, and VM ability VM was analyzed in glioma cells. The results are shown in Figures 2E–2H. Compared with the control group, the *PABPC5 (–) + HCG15 (–)-NC* group and the *PABPC5 (–) + HCG15 (+)-NC* group significantly inhibited proliferation, migration, invasion, and VM ability and reduced expression levels of *LAMC2* protein ($p < 0.01$ and $p < 0.05$); compared with the *PABPC5 (–) + HCG15 (–)-NC* group, the *PABPC5 (–) + HCG15 (–)* group had significantly inhibited glioma cell proliferation, migration, invasion, and VM formation and significantly reduced expression levels of *LAMC2* ($p < 0.01$ and $p < 0.05$). Compared with the *PABPC5 (–) + HCG15 (+)-NC* group, *HCG15 (+)* reversed the inhibitory effect of *PABPC5 (–)* on proliferation, migration, invasion, VM ability of VM and *LAMC2* protein expression in *PABPC5 (–) + HCG15 (+)* ($p < 0.01$ and $p < 0.05$).

Figure 1. Endogenous Expression of *PABPC5* and *HCG15* and the Effect of *PABPC5* and *HCG15* on the Biological Behavior of Glioma Cells

(A) *PABPC5* protein expression levels in normal brain tissue (NBT), low-grade glioma tissue (LGGT), and high-grade glioma tissue (HGGT). The protein expression and corresponding IDV values of *PABPC5* in NBT, LGGT, and HGGT are shown; the data are expressed as mean ± SD (n = 12). Compared with the NBT group, **p < 0.01; compared with the LGGT group, #p < 0.05. (B) *PABPC5* protein levels in normal human astrocytes (NHAs) and U87 and U251 cells. The protein expression and corresponding IDV values of *PABPC5* in NHAs and U87 and U251 cells are shown; the data are expressed as mean ± SD (n = 3). Compared with the NHA group, *p < 0.05. (C) The effect of knockdown of *PABPC5* on the ability of proliferation was measured with CCK-8 in U87 and U251 cells. Data are expressed as mean ± SD (n = 3). Compared with the *PABPC5 (–)-NC* group, *p < 0.05. (D) The effect of knockdown of PABPC5 on the migration and invasion ability of U87 and U251 cells by was tested by Transwell test. Representative images and corresponding statistical analysis diagrams are shown. Data are expressed as mean ± SD (n = 3). Compared with the *PABPC5 (–)-NC* group, **p < 0.01; the scale bar indicates 50 μm. (E) Three-dimensional culture was used to determine the effect of knockdown of PABPC5 on the VM formation ability of U87 and U251 cells. Representative images and corresponding statistical analysis plots are shown. Data are expressed as mean ± SD (n = 3). Compared with the *PABPC5 (–)-NC* group, **p < 0.01. The scale bar indicates 50 μm. (F) Knockdown of *PABPC5* regulates *LAMC2* protein expression levels in U87 and U251 cells. The data are expressed as mean ± SD (n = 3). Compared with the *PABPC5 (–)-NC* group, *p < 0.05 and **p < 0.01. (G) *HCG15* expression in NBT, LGGT, and HGGT. Data are expressed as mean ± SD (n = 12). Compared with the NBT group, **p < 0.01 and *p < 0.05. Compared with the LGGT group, #p < 0.05. (H) *HCG15* expression in NHAs and U87 and U251 cells. Data are expressed as mean ± SD (n = 3). Compared with the NHA group, **p < 0.01 and *p < 0.05. (I) detecting the effects of knockdown and overexpression of *HCG15* on proliferation. Data are expressed as mean ± SD (n = 3). Compared with the *HCG15 (–)-NC* group, **p < 0.01 and *p < 0.05. Compared with the *HCG15 (+)-NC* group, ##p < 0.01. (J) Detecting the effects of knockdown and overexpression of *HCG15* on the migration and invasion ability of U87 and U251 cells. Data are expressed as mean ± SD (n = 3). Compared with the *HCG15 (–)*-NC group, **p < 0.01. Compared with the *HCG15* (+)-NC group, ##p < 0.01. The scale bar indicates 50 μm. (K) Effect of knockdown and expression of *HCG15* on the VM formation ability of U87 and U251 cells. Data are expressed as mean ± SD (n = 3). Compared with the *HCG15 (–)-NC* group, **p < 0.01. Compared with the *HCG15 (+)-NC* group, ##p < 0.01 and #p < 0.05. The scale bar indicates 50 μm. (L) Detecting the effects of knockdown and overexpression of *HCG15* regulates *LAMC2* protein expressional levels in U87 and U251 cells, respectively. Data are expressed as mean ± SD (n = 3). Compared with the *HCG15 (–)-NC* group, **p < 0.01. Compared with the *HCG15 (+)-NC* group, ##p < 0.01.

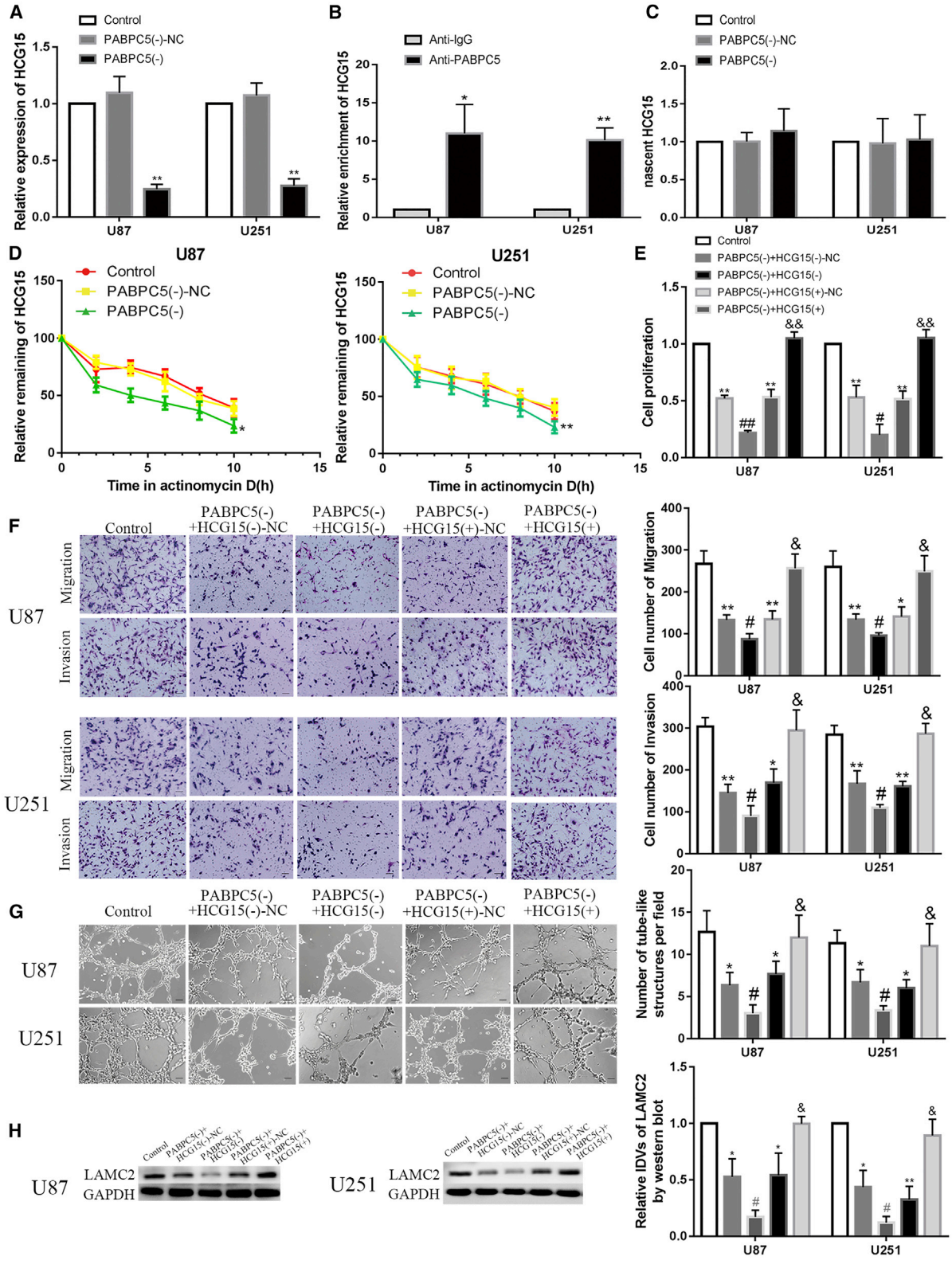

(legend on next page)

ZNF331 Was Lowly Expressed in Glioma Tissues and Cells, and Overexpression of *ZNF331* Inhibited VM Formation

Western blot was used to detect *ZNF331* expression in glioma tissues (12 normal brain tissues, 12 low-grade glioma tissues [WHO I–II], and 12 high-grade glioma tissues [WHO III–IV]) and in glioma cells (U87 and U251). As shown in Figures 3A and 3B, compared with the normal brain tissue group, the expression of *ZNF331* was significantly reduced in low-grade glioma tissue and high-grade glioma tissue ($p < 0.01$), and the expression of *ZNF331* was significantly lower than in low-grade glioma tissues ($p < 0.01$). In U87 and U251 glioma cells, the expression levels of *ZNF331* were significantly lower than in the NHA group ($p < 0.01$). The effects of *ZNF331* knockdown and overexpression on the biological behavior of gliomas were examined. Knockdown and overexpression of *ZNF331* were constructed in glioma cells. The tumor cells were tested for transfection efficiency. We selected #1 with the higher knockdown efficiency for subsequent experiments ($p < 0.01$) (Figure S1E). We tested the transfection efficiency of overexpressing *ZNF331* glioma cells . Its expression increased about three times ($p < 0.01$) (Figure S1F). The results are shown in Figures 3C–3F. Compared with the control group, no significant statistical difference was found between the *ZNF331 (–)-NC* group and the *ZNF331 (+)-NC* group. Compared with the *ZNF331 (–)-NC* group, the *ZNF331 (–)* group had significantly enhanced cell proliferation, migration, invasion, and VM formation ability and enhanced *LAMC2* protein expression levels ($p < 0.01$ and $p < 0.05$). Compared with the *ZNF331 (+)-NC* group, in the *ZNF331 (+)* group, proliferation, migration, invasion, and VM formation ability were significantly reduced, as were *LAMC2* protein expression levels ($p < 0.01$). After *PABPC5* knockdown in glioma cells, compared with the control group, there was no significant statistical difference between the *PABPC5 (–)-NC* group. Compared with the *PABPC5 (–)-NC* group, the expression of *ZNF331* mRNA and protein was significantly increased in the *PABPC5 (–)* group ($p < 0.01$ and $p < 0.05$). (Figure 3G). After knockdown and overexpression of *HCG15* in glioma cells, compared with the control group, there was no significant statistical difference between the *HCG15 (–)-NC* group and the *HCG15 (+)-NC* group. Compared with the *HCG15 (–)-NC* group, the expression of *ZNF331* mRNA and protein was significantly increased in the *HCG15 (–)* group ($p < 0.01$). Compared with the *HCG15 (+)-NC* group, the expression of *ZNF331* mRNA and protein was significantly reduced in the *HCG15 (+)* group ($p < 0.01$) (Figure 3H). The stable *PABPC5* knockdown cotransfection with *HCG15* knockdown or overexpression glioma cells were constructed. The effect on *ZNF331* mRNA and protein was examined. The results are shown in Figure 3I. Compared with the control group, the *PABPC5 (–)+HCG15 (–)-NC* group and *PABPC5 (–) + HCG15 (+)-NC* group had significantly increased mRNA and protein levels of *ZNF331* ($p < 0.01$ and $p < 0.05$). The *PABPC5 (–) + HCG15 (–)* group compared with the *PABPC5 (–) + HCG15 (–)-NC* group had significantly higher mRNA and protein expression levels of *ZNF331* ($p < 0.01$ and $p < 0.05$). Compared with the *PABPC5 (–) + HCG15 (+)-NC* group, *HCG15 (+)* reversed the inhibitory effect of *PABPC5 (–)* on the mRNA and protein expression of *ZNF331* in *PABPC5 (–) + HCG15 (+)* group($p < 0.01$ and $p < 0.05$).

HCG15 Promoted the Degradation of *ZNF331* and Enhanced the VM Formation of Glioma Cells through the SMD Pathway

By applying a bioinformatics database (IntaRNA), it was predicted that *HCG15* may bind to the 3′ UTR of *ZNF331* mRNA through a specific sequence Alu element. We applied a dual-luciferase gene reporting analysis system to verify this. Compared with the *ZNF331-3′UTR-Wt + HCG15 (+)-NC* group, the luciferase activity of the *ZNF331-3′UTR-Wt + HCG15(+)* group significantly decreased ($p < 0.05$), but there was no statistical difference between the *ZNF331-3′UTR-Mut + HCG15 (+)* group and the *ZNF331-3′UTR-Mut + HCG15 (+)-NC* group (Figure 4A). We applied RNA IP experiments to verify the relationship between *HCG15* and *STAU1*, *STAU1*, and *ZNF331*. We found that *HCG15* (*ZNF331* mRNA) was significantly higher in the anti-*STAU1* group than in the anti-IgG group ($p < 0.01$) (Figure 4B). To determine whether *STAU1* and *UPF1* participate in the interaction between *HCG15* and *ZNF331* mRNA, U87 and U251 cells were transfected with *STAU1* and *UPF1* knockdown plasmids. Nascent RNA experiments were performed; we found that the *HCG15 (–)-NC* group, *HCG15 (+) -NC* group, *STAU1 (–)-NC* group, and *UPF1 (–)-NC* group compared with the *HCG15 (–)* group, *STAU1 (–)* group, and *UPF1 (–)* group showed no significant statistical difference, meaning that there were no nascent *ZNF331* mRNA changes. In the *HCG15 (–)-NC* group, *STAU1 (–)-NC* group, and *UPF1 (–)-NC* group, the half-life of *ZNF331* mRNA was significantly longer than in the *HCG15 (–)* group, *STAU1 (–)* group, and *UPF1 (–)* group ($p < 0.01$ and $p < 0.05$). Compared

Figure 2. *PABPC5* Enhanced the Biological Behavior of Glioma Cells by Increasing the Stability of *HCG15*

(A) Knockdown of *PABPC5* affects *HCG15*. Data are expressed as mean ± SD (n = 3). Compared with the *PABPC5 (–)-NC* group, **$p < 0.01$. (B) Validating the binding interaction between *PABPC5* and *HCG15*. Data are expressed as mean ± SD (n = 3). Compared with the respective anti-normal IgG groups, **$p < 0.01$. (C) knockdown of *PABPC5* to detect nascent *HCG15* in U87 and U251 cells; data are expressed as mean ± SD (n = 3). (D) Effect of knockdown of *PABPC5* on *HCG15* half-life. Data are expressed as mean ± SD (n = 3). Compared with the *PABPC5 (–)-NC* group, **$p < 0.01$ and *$p < 0.05$. (E) Detecting the effects of knockdown of *PABPC5*, knockdown of *HCG15*, and overexpression of *HCG15* on the proliferation ability of U87 and U251 cells. Data are expressed as mean ± SD (n = 3). Compared with the control group, **$p < 0.01$. Compared with the *PABPC5 (–) + HCG15 (–)-NC* group, #$p < 0.05$ and ##$p < 0.01$. Compared with the *PABPC5 (–) + HCG15 (+)-NC* group, &&$p < 0.05$. (F) Detecting the effects of knockdown of *PABPC5*, knockdown of *HCG15*, and overexpression of *HCG15* on the migration and invasion ability of U87 and U251 cells. Data are expressed as mean ± SD (n = 3). Compared with the control group, *$p < 0.05$ and **$p < 0.01$. Compared with the *PABPC5 (–) + HCG15 (–)-NC* group, # $p < 0.05$. Compared with the *PABPC5 (–) + HCG15 (+)-NC* group, &$p < 0.05$. The scale bar indicates 50 μm. (G) Detecting the effects of knockdown of *PABPC5*, knockdown of *HCG15*, and overexpression *HCG15* on the VM ability of U87 and U251 cells. Data are expressed as mean ± SD (n = 3). Compared with the control group, *$p < 0.05$. Compared with the *PABPC5 (–) + HCG15 (–)-NC* group, #$p < 0.05$. Compared with the *PABPC5 (–) + HCG15 (+)-NC* group, &$p < 0.05$. The scale bar indicates 50 μm. (H) Detecting the effects of knockdown of *PABPC5*, knockdown of *HCG15*, and overexpression of *HCG15* on *LAMC2* protein expression in U87 and U251 cells. Data are expressed as mean ± SD (n = 3). Compared with the control group, *$p < 0.05$ and **$p < 0.01$. Compared with the *PABPC5 (–) + HCG15 (–)-NC* group, #$p < 0.05$. Compared with the *PABPC5 (–) + HCG15 (+)-NC* group, &$p < 0.05$.

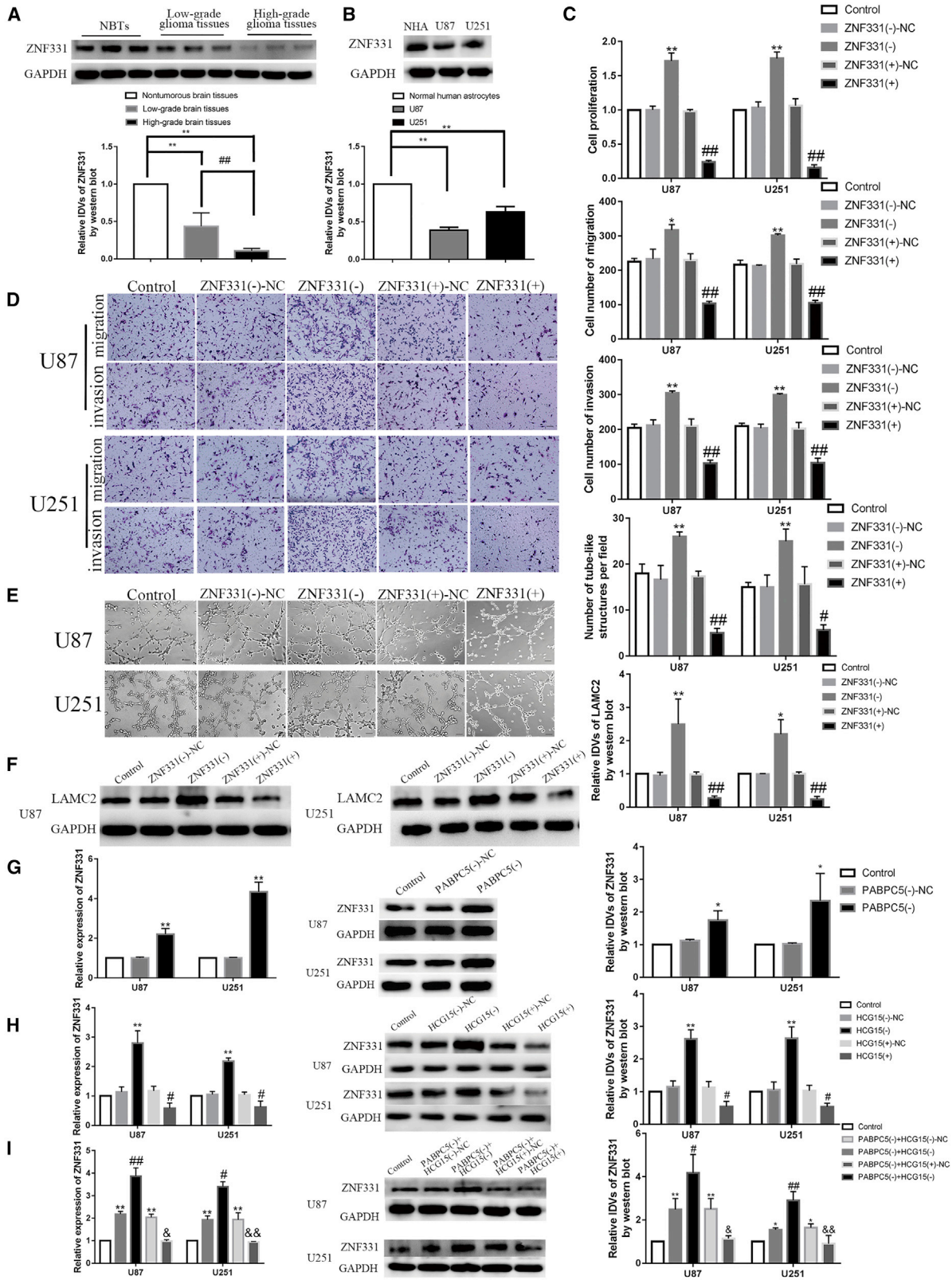

(legend on next page)

with the *HCG15 (+)-NC* group, the half-life of *ZNF331* mRNA was significantly reduced in the *HCG15 (+)* group ($p < 0.01$) (Figures 4C–4E). In addition, compared with the *STAU1 (–)-NC* and *UPF1 (–)-NC* groups, the protein expression of *ZNF331* was significantly increased in the *STAU1 (–)* and *UPF1 (–)* groups ($p < 0.01$ and $p < 0.05$) (Figures 4F and 4G). We further knocked down or overexpressed *STAU1* and knocked down *HCG15* in glioma cells and detected changes in *ZNF331* protein expression. The results are shown in Figure 4H. Compared with the control group, the expression levels of the *HCG15 (–) + STAU1 (–)-NC* group and *HCG15 (–) + STAU1 (+)-NC* group were significantly increased ($p < 0.01$ and $p < 0.05$). Compared with the *HCG15 (–) + STAU1 (–)-NC* group, the *HCG15 (–) + STAU1 (–)* group had significantly increased expression levels of *ZNF331* protein ($p < 0.01$ and $p < 0.05$). Compared with the *HCG15 (–) + STAU1 (+)-NC* group, *STAU1 (+)* significantly reversed the effect of *HCG15 (–)* on increasing the expression level of *ZNF331* in the HCG15 (–) + STAU1 (+) group ($p < 0.01$ and $p < 0.05$).

Furthermore, *ZNF331* was knocked down or overexpressed in glioma cells, which were transfected with *HCG15 (–)* at the same time. The results are shown in Figures 4I–4K. Compared with the *HCG15 (–)-NC + ZNF331 (+)-NC* group, the *HCG15 (–) +ZNF331 (+)* group had a stronger ability to inhibit glioma cell proliferation, migration, invasion, and VM formation ($p < 0.01$). Compared with the *HCG15 (–)-NC + ZNF331 (–)-NC* group, *HCG15 (–), ZNF331 (–)* reversed the inhibitory effect of *HCG15 (–)* in the *HCG15 (–) + ZNF331 (–)* group on glioma cell proliferation, migration, invasion, and VM formation. Western blot experiment results showed that, compared with the *HCG15 (–)-NC + ZNF331 (+)-NC* group, the *HCG15 (–) + ZNF331 (+)* group had significantly inhibited expression of *LAMC2* protein ($p < 0.01$). Compared with *HCG15 (–)-NC + ZNF331 (–)-NC*, *ZNF331 (–)* reversed the inhibitory effect of *HCG15 (–)* on the expression of *LAMC2* protein in the *HCG15 (–) + ZNF331 (–)* group (Figure 4L).

ZNF331 Bound Directly to the Promoter Regions of *LAMC2* and *PABPC5*

We predicted from the bioinformatics database (JASPAR) that *ZNF331* may have potential binding sites with the promoter regions (−2,000 ~ −1,000 bp) of *LAMC2* and *PABPC5*. Chromatin IP (ChIP) experiments verified that *ZNF331* combined with *LAMC2* and *PABPC5*. The results are shown in Figures 5A and 5B. *ZNF331* could be seen at the binding sites of *LAMC2* and *PABPC5*, which proved that there was binding in the promoter region. Interestingly, we found that *ZNF331* not only altered *LAMC2* but also affected *PABPC5*. *ZNF331* was knocked down or overexpressed in glioma cells. The changes in *LAMC2* mRNA and *PABPC5* mRNA were analyzed by real-time qPCR (Figures 5C and 5D). Compared with the control group, the *ZNF331 (–)-NC* group and *ZNF331 (+)-NC* group showed no significant statistical difference. Compared with the *ZNF331 (–)-NC* group, the expression of *LAMC2* and *PABPC5* mRNA was significantly increased in the *ZNF331 (–)* group ($p < 0.01$). Compared with the *ZNF331 (+)-NC* group, *LAMC2* and *PABPC5* mRNA expression was significantly reduced in the *ZNF331 (+)* group ($p < 0.01$ and $p < 0.05$). In previous experiments, we detected that *ZNF331* regulated the expression of *LAMC2* protein and affected the ability of VM formation. This time we also used knockdown and overexpression of *ZNF331* glioma cells to detect the expression of *PABPC5* protein. The results are shown in Figure 5E. Compared with the control group, the *ZNF331 (–)-NC* group and *ZNF331 (+)-NC* group had no significant statistical difference. Compared with the *ZNF331 (–)-NC* group, the protein expression of *PABPC5* was significantly increased in the *ZNF331 (–)* group ($p < 0.01$ and $p < 0.05$). Compared with the *ZNF331 (+)-NC* group, the protein expression of *PABPC5* was significantly decreased in the *ZNF331 (+)* group ($p < 0.01$ and $p < 0.05$).

Knockdown of *PABPC5* and *HCG15* and Overexpression of *ZNF331* Alone or in Combination Inhibited Glioma Growth and Prolonged the Survival Time of Nude Mice

The above hypothesis was confirmed by *in vivo* tumor model experiments. First, subcutaneous transplantation tumor technology was used to clarify the effects of *PABPC5* knockdown, *HCG15* knockdown, and overexpression of *ZNF331* on glioma growth volume alone or in combination (Figures 6A and 6B). There was no significant difference between the control group and the negative control (NC) group. Compared with the NC group, *PABPC5 (–)* group, *HCG15*

Figure 3. *ZNF331* Was Lowly Expressed in Gliomas and Inhibited the Formation of Vascular Mimicry

(A) *ZNF331* protein expression levels in NBT, LGGT, and HGGT. Data are expressed as mean ± SD (n = 12). Compared with the NBT group, **p < 0.01. Compared with the LGGT group, ## p < 0.01. (B) *ZNF331* protein expression levels in NHAs and U87 and U251 cells. Data are expressed as mean ± SD (n = 3). Compared with the NHA group **p < 0.01. (C) Detecting the effects of knockdown and overexpression of *ZNF331* on the proliferation ability of U87 and U251 cells. Data are expressed as mean ± SD (n = 3). Compared with the *ZNF331 (–)-NC* group, **p < 0.01. Compared with the *ZNF331 (+)-NC* group, ##p < 0.01. (D) Detecting the effect of *ZNF331* on the migration and invasion ability of U87 and U251 cells. Data are expressed as mean ± SD (n = 3). Compared with the *ZNF331 (–)-NC* group, *p < 0.05 and **p < 0.01. Compared with the *ZNF331 (+)-NC* group, ##p < 0.01. The scale bar indicates 50 μm. (E) Detecting the effects of *ZNF331* on the VM formation ability of U87 and U251 cells. Data are expressed as mean ± SD (n = 3). Compared with the *ZNF331 (–)-NC* group, **p < 0.01. Compared with the *ZNF331 (+)-NC* group, #p < 0.05 and ##p < 0.01. The scale bar indicates 50 μm. (F) Detecting the effects of knockdown and overexpression of *ZNF331* regulates *LAMC2* protein expressional levels in U87 and U251 cells, respectively. Data are expressed as mean ± SD (n = 3). Compared with the *ZNF331 (–)-NC* group, **p < 0.01 and *p < 0.05. Compared with the *ZNF331 (+)-NC* group, ##p < 0.01. (G) Expression levels of *ZNF331* mRNA and protein are detected in U87 and U251 cells after knockdown of *PABPC5*. Data are expressed as mean ± SD (n = 3). Compared with the *PABPC5 (–)-NC* group, *p < 0.05 and **p < 0.01. (H) The expression levels of *ZNF331* mRNA and protein are detected in U87 and U251 cells after knockdown and overexpression of *HCG15*. Data are expressed as mean ± SD (n = 3). Compared with the *HCG15 (–)-NC* group, **p < 0.01. Compared with the *HCG15 (+)-NC* group, #p < 0.05. (I) Expression levels of *ZNF331* mRNA and protein in U87 and U251 cells after knockdown of *PABPC5*, knockdown of *HCG15*, and overexpression of *HCG15*. Data are expressed as mean ± SD (n = 3). Compared with the control group, *p < 0.05 and **p < 0.01. Compared with the *PABPC5 (–) + HCG15 (–)-NC* group, #p < 0.05 and ##p < 0.01. Compared with the *PABPC5 (–) + HCG15 (+)-NC* group, &p < 0.05 and &&p < 0.01.

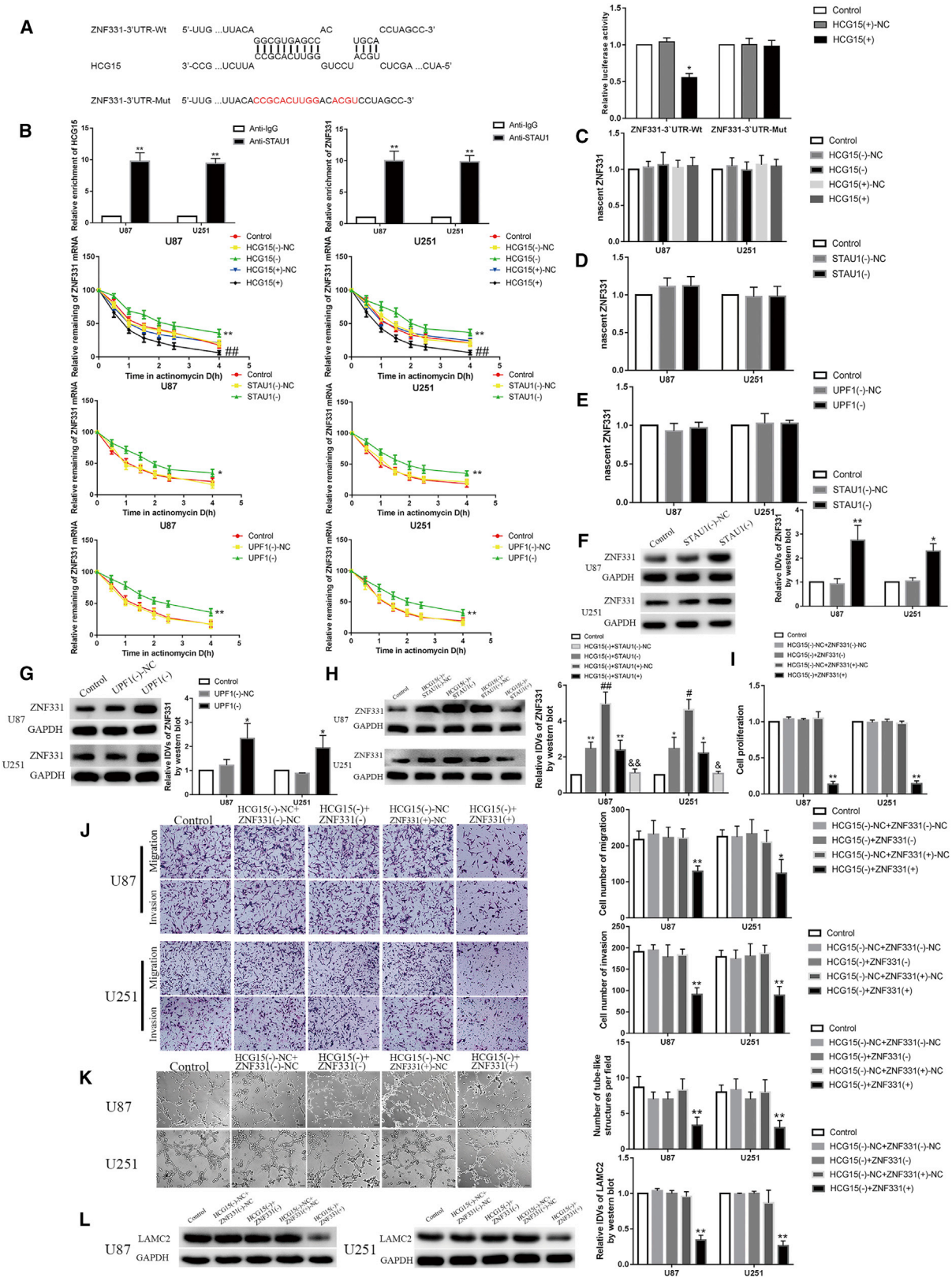

(legend on next page)

(–) group, *ZNF331 (+)* group, and *PABPC5 (–) + HCG15 (–) + ZNF331 (+)* group tumor volumes were significantly lower ($p < 0.01$). No significant difference was found between the *PABPC5 (–)* group, *HCG15 (–)* group, and *ZNF331 (+)* group. Compared with the *PABPC5 (–)* group, *HCG15 (–)* group, and *ZNF331 (+)* group, the *PABPC5 (–) +HCG15 (–) +ZNF331 (+)* group had the most obvious effect of lower tumor volume ($p < 0.01$). The effect of *PABPC5* knockdown, *HCG15* knockdown, and *ZNF331* overexpression on the survival time of nude mice was studied using orthotopic transplantation tumor technology (Figure 6C). There was no significant statistical difference between the control group and the NC group. Compared with the NC group, the *PABPC5 (–)* group, *HCG15 (–)* group, *ZNF331 (+)* group, and *PABPC5 (–) + HCG15 (–) + ZNF331 (+)* group had significantly longer survival times ($p < 0.01$ and $p < 0.05$). No significant difference was found between the *PABPC5 (–)* group, *HCG15 (–)* group, and *ZNF331 (+)* group. Compared with the *PABPC5 (–)* group, *HCG15 (–)* group, and *ZNF331 (+)* group, the *PABPC5 (–) + HCG15 (–) + ZNF331 (+)* group had the longest survival time. Finally, we wanted to clearly show whether there was a statistical difference in the number of VMs among the group. Subcutaneously transplanted tumors in nude mice were surgically excised, and the tumor tissues were sectioned with CD34-PAS dual staining. IHC was used for VM detection. No significant difference was found between the control group and the NC group. Compared with the NC group, the number of VMs in the *PABPC5 (–)* group, *HCG15 (–)* group, *ZNF331 (+)* group, and *PABPC5 (–) +HCG15 (–) +ZNF331 (+)* group were reduced significantly ($p < 0.01$ and $p < 0.05$). No significant difference was found between the *PABPC5 (–)* group, *HCG15 (–)* group, and *ZNF331 (+)* group. Compared with the *PABPC5 (–)* group, *HCG15 (–)* group, and *ZNF331 (+)* group, the number of VMs was significantly reduced in the *PABPC5 (–) + HCG15 (–) + ZNF331 (+)* group ($p < 0.05$) (Figure 6D).

DISCUSSION

This is the first study to verify that *PABPC5* and *HCG15* are highly expressed in glioma tissues and cells. In glioma cell knockdown, *PABPC5* inhibits proliferation, migration, invasion, and VM formation by reducing the stability of *HCG15*. *ZNF331* is lowly expressed in glioma tissues and cells. Knockdown of *HCG15* inhibits degradation of *ZNF331* mRNA through the SMD pathway and increases the expression of *ZNF331* in glioma cells to inhibit the malignant biological behavior of glioma cells and formation of VM. *ZNF331* not only directly binds to the *LAMC2* promoter region of VM-related proteins but also binds to the promoter region of *PABPC5*. At the same time, *ZNF331* plays the role of transcription repressor; it inhibits transcription of *PABPC5* and *LAMC2*. *PABPC5*, *HCG15*, and *ZNF331* construct a feedback loop to regulate VM formation (Figure 6E).

RBPs play an important role in regulating the formation of VM of tumor cells by binding to single- or double-stranded RNA.[35] *RBP-BNIP3* is highly expressed in melanoma cells, and RBP-BNIP3 binds to *CD47*; it induces VM formation in the cell's hypoxic state and mediates cell adhesion and migration of extracellular matrix.[36] *Fus* is highly expressed in glioma tissues and cells, and knockdown of *Fus* inhibits formation of glioma cell VM through the feedback regulation loop formed by *circ_002136/miR-138-5p/SOX13*.[37] This study found that *PABPC5* was highly expressed in glioma tissues and cells and that knockdown of *PABPC5* inhibited proliferation, migration, invasion, and VM formation of glioma cell. At the same time, *PABPC5* inhibited expression of the VM marker protein *LAMC2* protein level. That indicates that *PABPC5* plays an oncogenic role in glioma cells.

Recent studies have demonstrated that lncRNAs are abnormally expressed in a variety of tumors;[38] they are involved in regulation of tumorigenesis and development.[39,40] The lncRNA *HOXA-AS2* is highly expressed in glioma tissues and cells, and its expression is inhibited by binding to *miR-373*. It increases the expression of *EGFR* and promotes VM of glioma cells.[41] At the same time, the lncRNA *MIR155HG* promotes the growth of glioma cells through the *miR-185/ANXA2* axis.[42] Our previous work found that *HCG15* is highly expressed in glioma tissues and cells. Knockdown of *HCG15* reduced the expression level of *LAMC2* protein and inhibited the proliferation, migration, invasion, and VM formation of glioma cells. Overexpression of *HCG15* increased the protein expression level of *LAMC2* and promoted malignant biological behavior of glioma cells. It has been suggested that *HCG15* plays a tumor-promoting role in glioma cells.

Figure 4. *HCG15* Degraded *ZNF331* mRNA through the SMD Pathway, Enhancing the Biological Behavior of Glioma Cells

(A) Predicted results of *HCG15* binding site and dual-luciferase reporter gene assays in the 3′ UTR of *ZNF331* mRNA. Data are expressed as mean ± SD (n = 3). Compared with the *ZNF331-3′UTR-Wt + HCG15 (+)-NC* group, *p < 0.05. (B) RNA IP results. Data are expressed as mean ± SD (n = 3). Compared with the anti-normal IgG group, **p < 0.01. (C) The effect of *HCG15* on the stability of *ZNF331* mRNA; the data are expressed as mean ± SD (n = 3). Compared with the *HCG15 (–)-NC* group, **p < 0.01. Compared with the *HCG15 (+)-NC* group, ##p < 0.01. (D) *STAU1* effects on the stability of *ZNF331* mRNA; data are expressed as mean ± SD (n = 3). Compared with the *STAU1 (–)-NC* group, *p < 0.05 and **p < 0.01. (E) The effect of *UPF1* on the stability of *ZNF331* mRNA; data are expressed as mean ± SD (n = 3). Compared with the *UPF1 (–)-NC* group, *p < 0.05 and **p < 0.01. (F) Effect of *STAU1* on *ZNF331* protein expression; data are expressed as mean ± SD (n = 3). Compared with the *STAU1 (–)-NC* group, *p < 0.05 and **p < 0.01. (G) Effect of *UPF1* on *ZNF331* protein expression; data are expressed as mean ± SD (n = 3). Compared with the *UPF1 (–)-NC* group, *p < 0.05. (H) Effect of *HCG15* and *STAU1* on *ZNF331* protein expression; data are expressed as mean ± SD (n = 3). Compared with the control group, *p < 0.05 and **p < 0.01. Compared with the *HCG15 (–) + STAU1 (–)-NC* group, # p < 0.05 and ## p < 0.01. Compared with the *HCG15 (–)+ STAU1 (+)-NC* group, &p < 0.05 and &&p < 0.01. (I) Detecting the effects of *HCG15* and *ZNF331* on the proliferation ability of U87 and U251 cells. Data are expressed as mean ± SD (n = 3). Compared with the *HCG15 (–)-NC + ZNF331 (+)-NC* group, **p < 0.01. (J) Examining the effects of *HCG15* and *ZNF331* on the migration and invasion ability of U87 and U251 cells. Data are expressed as mean ± SD (n = 3). Compared with the *HCG15 (–)-NC + ZNF331 (+)-NC* group, **p < 0.01 and *p < 0.05. The scale bar indicates 50 μm. (K) Detecting the effects of *HCG15* and *ZNF331* on the VM formation ability of U87 and U251 cells. Data are mean ± SD (n = 3). Compared with the *HCG15 (–) + ZNF331 (+)-NC* group, **p < 0.01. The scale bar indicates 50 μm. (L) Detecting the regulation of *LAMC2* protein expression in U87 and U251 cells by *HCG15* and *ZNF331*. Data are expressed as mean ± SD (n = 3). Compared with the *HCG15 (–)-NC + ZNF331 (+)-NC* group, **p < 0.01.

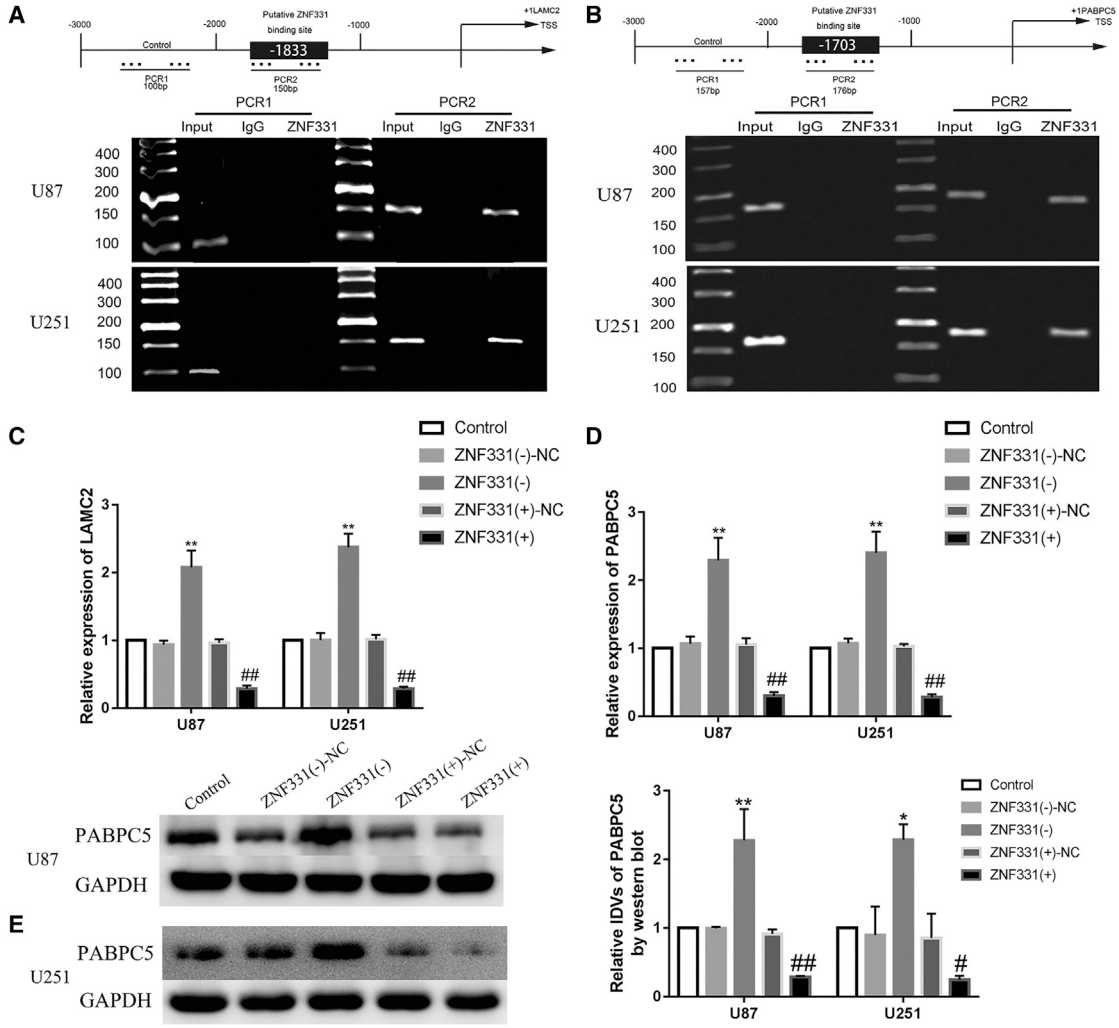

Figure 5. *ZNF331* Bound to the Promoter Regions of *LAMC2* and *PABPC5*

(A) *ZNF331* binds to the promoter of *LAMC2*. Shown is a schematic diagram of the 2,000-bp *LAMC2* promoter region upstream of the transcription start site (TSS), which is designated as +1. The putative *ZNF331* binding site is shown. Using rabbit IgG as an NC, PCR was used to amplify the immunoprecipitated DNA. (B) *ZNF331* binds to the promoter of *PABPC5*. Shown is a schematic diagram of the 2,000-bp *PABPC5* promoter region upstream of the TSS, which is designated as +1. The putative *ZNF331* binding site is shown. Using rabbit IgG as an NC, PCR was used to amplify the immunoprecipitated DNA. (C) *ZNF331* effect on *LAMC2* mRNA expression. Data are expressed as mean ± SD (n = 3). Compared with the *ZNF331 (–)-NC* group, **p < 0.01. Compared with the *ZNF331 (+)-NC* group, ##p < 0.01. (D) *ZNF331* effects on expression of *PABPC5* mRNA. Data are expressed as mean ± SD (n = 3). Compared with the *ZNF331 (–)-NC* group, **p < 0.01. Compared with the *ZNF331 (+)-NC* group, ##p < 0.01. (E) *ZNF331* affects the expression of *PABPC5* protein. Data are expressed as mean ± SD (n = 3). Compared with the *ZNF331 (–)-NC* group, **p < 0.01 and *p < 0.05. Compared with the *ZNF331 (+)-NC* group, ## p < 0.01.

We previously reported the mechanisms of various lncRNAs regulating the formation of glioma cell VM. For example, *SNHG16* and *USF1* are highly expressed in glioma tissues and cells and play a role in promoting VM formation by combining *miR-212-3p* and *miR-429*.[43] *TUG1* plays the role of an oncogenic gene through negatively regulating the effect of *miR-299* and enhancing angiogenesis in tumors.[44]

Numerous studies have confirmed that RBPs regulate their stability by binding to lncRNAs and participate in the development of tumors.[45] *HuR* directly combines with *HOTAIR* to enhance its stability, which negatively regulates the expression of *miR-7* and promotes migration and invasion in head and neck squamous cell carcinoma cells.[46] In this study, a bioinformatics database RBP map search revealed that *PABPC5* and *HCG15* had potential binding sites. RNA IP experiments were used to verify this specific binding effect. Furthermore, we found that the expression level of *HCG15* was decreased after *PABPC5* knockdown in glioma cells, whereas the nascent *HCG15* was not transcribed but the half-life of *HCG15* was shortened. In other words, *HCG15* stability was

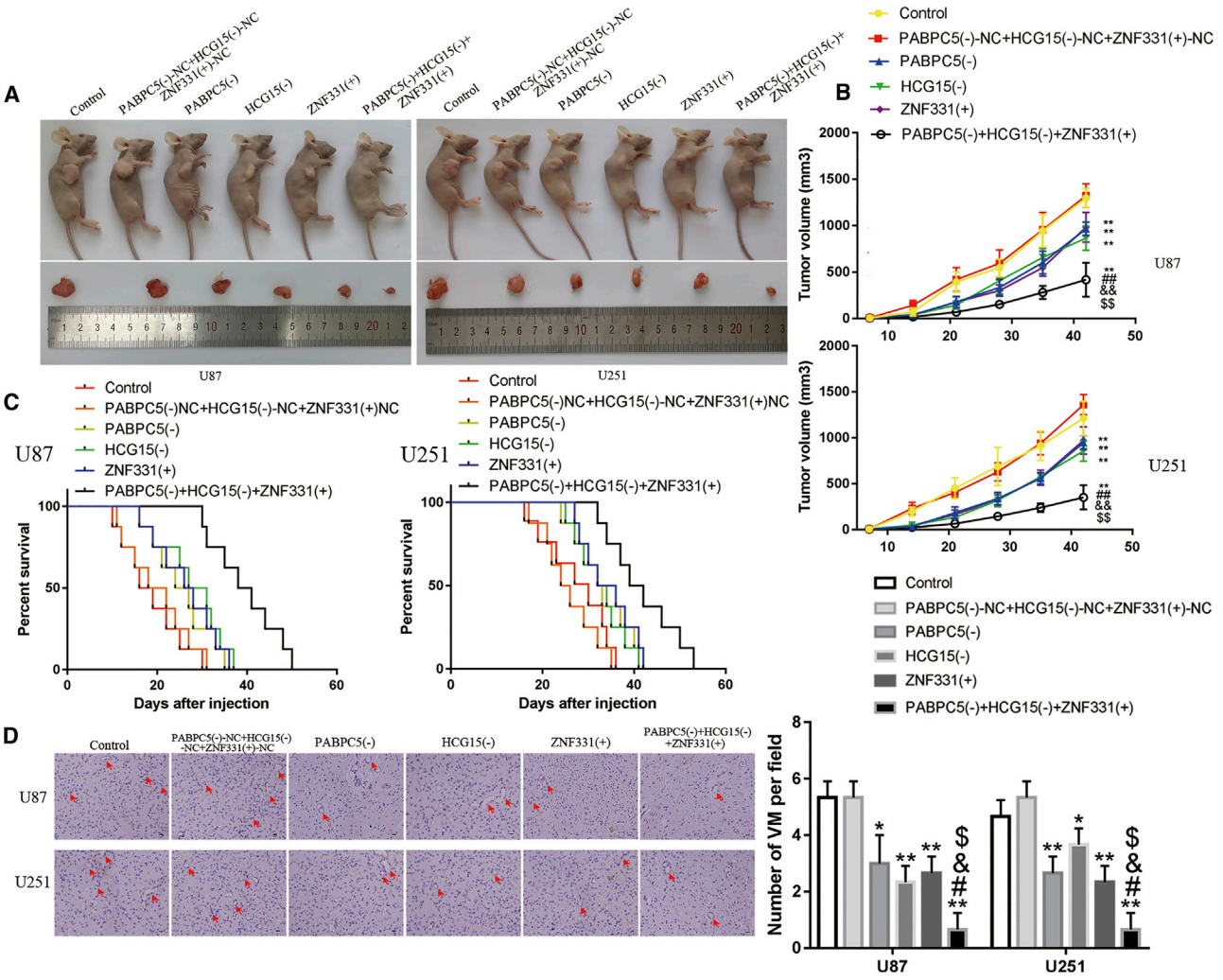

Figure 6. Tumor Xenograft Studies *In Vivo* Using Stably Transfected Cells

(A) Nude mouse samples and tumors from each group of subcutaneous xenograft tumors. (B) Curve of the volume of subcutaneous xenografts in nude mice. Tumor volume was calculated every 5 days after injection, and tumors were excised 45 days after transplantation; data are expressed as mean ± SD (n = 8). Compared with the *PABPC5 (–)-NC + HCG15 (–)-NC + ZNF331 (+)-NC* group (i.e., the NC group), **p < 0.01. Compared with the *PABPC5 (–)* group, ##p < 0.01. Compared with the *HCG15 (–)* group, &&p < 0.01. Compared with the *ZNF331 (+)* group, $$p < 0.01. (C) Intracranial orthotopic tumor implantation survival curve for nude mice (n = 8). (D) Detecting changes in the number of VMs in xenograft tumors; data are expressed as mean ± SD (n = 5). Compared with the *PABPC5 (–)-NC + HCG15 (–)-NC + ZNF331 (+)-NC* group (i.e., the NC group), *p < 0.05 and **p < 0.01. Compared with the *PABPC5 (–)* group, #p < 0.05. Compared with the *HCG15 (–)* group, &p < 0.05. Compared with the *ZNF331 (+)* group, $p < 0.05. The scale bar indicates 25 μm. (E) Interaction mechanism of *PABPC5*, *HCG15*, and *ZNF331* in gliomas.

reduced. Therefore, the stability of *HCG15* was changed by knockdown of *PABPC5*, which was not caused by *HCG15* nascent RNA. When knockdown of *PABPC5* was combined with knockdown of *HCG15*, the effect was strengthened further regarding proliferation, migration, invasion, and VM formation ability in glioma cells. Overexpression of *HCG15* reversed the inhibitory effect of *PABPC5* on the proliferation, migration, invasion, and VM formation ability of glioma cells.Therefore, *PABPC5* bound *HCG15* to regulate ability of VM formation by changing stability of *HCG15* in glioma cells.

ZNF331 plays a transcriptional inhibitory role in tumorigenesis and development.[47] *ZNF331* was originally identified in thyroid tumors; it is a member of the KRAB zinc-finger protein family and has a transcriptional regulatory function as a transcription repressor.[48] *ZNF331* inhibits the growth of esophageal and gastric cancers,[29,47] and other studies have found that *ZNF331* inhibits colony formation and cell proliferation in colorectal cancer cells and induces G1/S arrest during development of colorectal cancer. Because the *ZNF331* promoter region is often methylated, it loses its role as a tumor suppressor gene, so *ZNF331* plays a tumor-suppressive role in colon cancer.[49] This study

found that *ZNF331* was lowly expressed in glioma tissues and cells and that its expression level decreased as the glioma tissue pathological grade increased. Overexpression of *ZNF331* reduced the expression level of *LAMC2* protein and inhibited proliferation, migration, invasion, and VM formation ability in glioma cells.

The SMD pathway is ubiquitous in mammalian cell development.[50] It has been reported that lncRNAs bind to the 3′ UTR of transcription factors via Alu elements to form an SBS. After binding to *STAU1*, it directly recruits the ATP-dependent RNA helicase *UPF1* to trigger *STAU1*-mediated mRNA degradation.[51] The SMD pathway participates in a variety of cellular life processes, including differentiation of mouse myoblasts into myotubes[52] and differentiation of mouse adipocytes,[53] and can regulate the migration of human *HaCaT* keratinocytes.[51] *STAU1,* as a post-transcriptional regulator, function with lncRNA , and then they are involved in epidermal end differentiation in gastric cancer cell lines[54,55] and regulat cyclin-dependent kinase genestranscription and expression, thereby affecting the proliferation and apoptosis of gastric cancer cells..[56] In this study, the bioinformatics software Repeat Masker and IntaRNA were used to predict that there were Alu elements in *HCG15* and *ZNF331* and that there was a potential binding site between the Alu element of *HCG15* and the 3′ UTR of *ZNF331*. Dual-luciferase reporter gene and RNA IP experiments were used to verify this targeted binding effect and the binding site. We found that knockdown of *HCG15* significantly increased the expression level of *ZNF331* mRNA and extended its half-life. Overexpression of *HCG15* significantly reduced the expression level of *ZNF331* mRNA and shortened its half-life. Whereas the tanscription of nacsent *ZNF331* mRNA was not affected by *HCG15* , so *HCG15* combined with *ZNF331* via Alu to form SMD to change its stability. In the SMD pathway, *STAU1* binds to SBS formed in combination of lncRNA and target mRNA through Alu elements, and then recruits *UPF1* to play a role in post-translational modification.[57] Therefore, we knocked down *STAU1* and *UPF1* in glioma cells. We observed that each increased the expression level of *ZNF331* mRNA and extend its half-life to increase its stability and inhibit *LAMC2* expression, inhibiting formation of VM in glioma cells. Simultaneous knockdown of *HCG15* and *STAU1* further reduced the protein expression of *ZNF331*. Overexpression of *STAU1* reversed knockdown of *HCG15*, which increased *ZNF331* protein expression. This proved the interaction between *HCG15* and *STAU1*. Therefore, it was suggested that *HCG15* regulates the expression level of *ZNF331* by participating in the *STAU1*-mediated mRNA decay mechanism and then regulates VM formation. lncRNAs participate in molecular regulatory networks through the SMD pathway, which has attracted increasing attention from researchers. The lncRNA *SNHG5* is highly expressed in colorectal cancer cells, and knockdown of *SNHG5* blocks *STAU1*-mediated decay of *SPATA2* mRNA and inhibits growth of colorectal cancer cells through the SMD pathway.[58]

It is well known that *LAMC2* is a VM formation-related protein, and involved in the biological process of tumor vascular mimic formation.[34] The transcription factor *EphA2* activates the AKT pathway in high-serum-treated prostate cancer cells to increase the expression of *MMP-2* and *LAMC2*, increasing VM formation ability.[59] *ZEB1* binds directly to the *LAMC2* promoter region to exert transcriptional repression, so *ZEB1* inhibits migration and invasion of prostate cancer cells.[60] Studies have reported that low expression of *EphA2* or *LAMC2* inhibits VM formation in glioma cells.[61,62] In this study, ChIP experiments were performed to confirm the specific binding and binding sites of *ZNF331* and *LAMC2* promoter region. Knockdown of *ZNF331* increased the expression levels of *LAMC2* mRNA and protein, and the proliferation, migration, invasion, and VM formation ability of glioma cells was significantly enhanced, suggesting that *ZNF331* acts as a transcriptional repressor in gliomas to regulate VM formation. Further, the ChIP experiment was used to confirm that *ZNF331* had a binding effect and binding site with the promoter region of the upstream RBP *PABPC5*, and knockdown of *ZNF331* also increased *PABPC5* mRNA and protein expression levels. *ZNF331/PABPC5* formed a feedback loop to play an important role in regulating the formation of glioma VM.

Finally, in this study, knockdown of *PABPC5*, knockdown of *HCG15*, and overexpression of *ZNF331* were performed alone or in combination in nude mice. It was confirmed that knockdown of *PABPC5*, knockdown of *HCG15*, and overexpression of *ZNF331* alone could effectively inhibit the growth of transplanted tumors and prolong the survival of nude mice. Combined knockdown of *PABPC5*, knockdown of *HCG15*, and overexpression of *ZNF331* had the best antitumor effect and the longest survival time in nude mice. The potential value of *PABPC5* knockdown, *HCG15* knockdown, and *ZNF331* overexpression alone or association was suggested.

In summary, this study demonstrates, for the first time, that *PABPC5* and *HCG15* are highly expressed in glioma tissues and cells, that *PABPC5* and *HCG15* are targeted for binding, that *HCG15* acts on *ZNF331* through SMD, and that *ZNF331* is lowly expressed in glioma tissues and cells. Knockdown of *PABPC5* reduced the stability of *HCG15*, and knockdown of *HCG15* is through the SMD pathway to prevent its degradation of *ZNF331* mRNA. *ZNF331* binds to the *LAMC2* promoter region, inhibiting downstream *LAMC2* transcription and, thus, inhibiting glioma cell VM formation ability. *ZNF331* combines with the promoter region of *PABPC5* and inhibits upstream *PABPC5* transcription to form a feedback regulatory loop. Therefore, they inhibit the effects of proliferation, migration, invasion, and VM formation in glioma cell. The purpose of this study is to demonstrate that the *PABPC5/HCG15/ZNF331* feedback loop plays an important role in regulating glioma VM formation. The feedback loop provides new strategies for glioma treatment and new directions for glioma intervention.

MATERIALS AND METHODS

Cell Lines and Cell Culture

The glioma cell lines U87 and U251 and the human embryonic kidney 293T (HEK293T) cells were purchased from the Cell Resource Center of the Shanghai Institute of Biological Sciences. Primary NHAs were purchased from Sciencell Research Laboratory. The cells were

cultured in DMEM or RPMI 1640 medium (Gibco, Carlsbad, CA, USA) in 5% CO_2 and 37°C incubators.

Human Tissue Specimens

Normal brain tissue (NBT; n = 12) was selected as an NC for patients with traumatic craniocerebral trauma and craniotomy; gliomas and surgical patients were selected according to pathologists to determine the pathological grade according to WHO classification. All glioma tissues were classified into low-grade glioma (WHO I–II, n = 12) and high-grade glioma (WHO III–IV, n = 12). The above tissues were obtained from patients at Shengjing Hospital affiliated with China Medical University. All patients voluntarily provided signed informed consent. Human tissue specimens were approved by the hospital ethics committee.

CD34-Labeled Endothelium PAS Dual Staining

VM was detected by CD34-PAS in glioma tissues. The assay was performed as reported previously.[63]

Real-Time qPCR

The real-time qPCR assay was performed as reported previously.[63] The expression levels were normalized to endogenous controls, and the relative quantification of the RNA was expressed by the $2^{-\Delta\Delta Ct}$ method. The PCR primer sequences are shown in Table S1.

Cell Proliferation Assay

Cell viability was detected using CCK-8 (Beyotime Biotechnology, China). The process of preformation and application reagents were consistent with a previous report.[63]

Plasmid Construction and Cell Transfection

PABPC5 short hairpin RNA (*PABPC5(–)*), *HCG15* short hairpin RNA (*HCG15(–)*), the *HCG15* full-length plasmid (*HCG15(+)*), *ZNF331* short hairpin RNA (*ZNF331(–)*), the *ZNF331* full-length plasmid (*ZNF331(+)*), *STAU1* short hairpin RNA (*STAU1(–)*), the *STAU1* full-length plasmid (*STAU1(+)*), *UPF1* short hairpin RNA (*UPF1(–)*), and their respective non-targeting sequences (NC) were synthesized (GeneChem, Shanghai, China). Reagents for transfection systems and drugs for screening cells were identical to a previous report.[63] The plasmid sequences are shown in Table S2.

Western Blot

This procedure and the reagents used were consistent with a previous report.[63] The primary antibodies were as follows: *PABPC5* (1:500, abclonal, Wuhan, China), *ZNF331* (1:2,000, Proteintech, Rosemont, IL, USA), *LAMC2* (1:500, Santa Cruz Biotechnology, USA), and *GAPDH* (1:10,000, Proteintech, Rosemont, IL, USA). The secondary antibodies were diluted (1:10,000, Proteintech, Rosemont, IL, USA); *PABPC5*, *ZNF331*, and *LAMC2* were rabbit resistance, and *GAPDH* was mouse resistance. The ratio of the IDV(Integrated Density Value) integral density of the target band to the *GAPDH* band was used as the relative expression level of the target protein, and statistical analysis was performed.

Cell Migration and Invasion Assay

Cell migration and invasion were measured using a polycarbonate membrane with a pore size of 8 μm (Corning Life Sciences, NY, USA) in a 24-well chamber. Specific operational details have been described previously.[63]

In Vitro VM Tube Formation Assay

Each well was covered with 300 μL Matrigel (Becton Dickinson, Franklin Lakes, NJ, USA) in a 24-well plate, which was placed on a flat surface for coagulation. Specific operational details have been described previously.[63] Independent observers calculated the total number of tubular structures for each image for statistical analysis.

ChIP Assays

ChIP assays were performed using the Simple ChIP Enzymatic Chromatin IP Kit (Cell Signaling Technology, Danvers, MA, USA) according to the manufacturer's instructions. Specific operational details have been described previously.[63] The primer sequence is shown in Table S3.

Reporter Vector Construct and Luciferase Reporter Gene Assay

HEK293T cells were seeded in 96-well plates and co-transfected with the *ZNF3311-3′UTR-Wt* (or *ZNF331-3′UTR-Mut*) reporter plasmid and *HCG15(+)-NC* or *HCG15(+)*, respectively. The Dual-Luciferase Reporter Assay Kit (Promega) was used according to a previous report.[63]

RNA IP

RNA IP assays were performed using the EZ-Magna RNA-Binding Protein Immunoprecipitation Kit (Millipore, USA) according to the manufacturer's protocol. Specific operational details have been described previously.[63]

Nascent RNA Capture

Nascent RNA was detected using the Click-iT Nascent RNA Capture Kit (Thermo Fisher Scientific, USA) according to the manufacturer's protocol. Nascent RNA was labeled with 0.2 mM 5-ethyluridine (EU), and EU-neo RNA was captured on magnetic beads, followed by real-time qPCR detection.

mRNA Stability Assay

U87 and U251 cells were cultured separately, and the cell density was approximately 60%–80%. 5 μg/mL actinomycin D (ActD, NobleRyder, China) was added to the cell culture medium to inhibit *de novo* synthesis of RNA. The half-life of *HCG15* was determined at 0, 2, 4, 6, 8, and 10 h. *ZNF331* mRNA was extracted at 0, 0.5, 1, 1.5, 2, 2.5, and 4 h. The RNA was detected by real-time qPCR.

In Vivo Xenograft Mouse Model

For *in vivo* xenograft experiments, 4-week-old athymic nude mice (BALB/c) were purchased from the Cancer Institute of the China Academy of Medical Science, and the mice were randomly divided into 5 groups: a control group and *PABPC5(–)-NC*+*HCG15(–)-NC*+*ZNF331(+)-NC*, *PABPC5(–)*, *HCG15(–)*, *ZNF331(+)*, and *PABPC5(–)* +*HCG15(–)* +*ZNF331(+)* groups. When subcutaneous

xenografts were administered to each nude mouse, 3×10^5 glioma cells were injected into the right axillary area. According to the estimation formula,[63] tumor volume was measured every 7 days after implantation until 42 days after implantation. Finally, the presence of VM was detected by CD34-PAS dual stain. Survival analysis experiments were performed using a Kaplan-Meier survival curve. 3×10^5 glioma cells were injected into the right striatum by stereotactic technique, and the survival time was recorded. All experiments with mice were conducted strictly in accordance with the China Medical University Application for Laboratory Animal Welfare and Ethical Review (201702 Edition), approved by the Ethics Committee of China Medical University.

Statistical Analysis

All statistical analyses were performed using GraphPad Prism 7.0 (GraphPad, La Jolla, CA, USA) and SPSS 19.0 software (IBM, New York, NY, USA). All values were derived from the mean ± standard deviation (SD) of more than three independent experiments. The above results were analyzed by Student's t test or one-way analysis of variance (ANOVA). There was a statistically significant difference (at least $p < 0.05$).

SUPPLEMENTAL INFORMATION

Supplemental Information can be found online at https://doi.org/10.1016/j.omto.2020.03.017.

AUTHOR CONTRIBUTIONS

Y.L. contributed to experiment design, manuscript draft, and data analysis. F.J. contributed to experiment implementation, manuscript draft, and data analysis. Y.X. designed the experiments. X.R., C.Y., D.W., and S.S. performed the experiments. Y.Y. and L.S. analyzed the data. J.Z., P.W., X.L., and J.M. conceived or designed the experiments, performed the experiments, and wrote the manuscript. All authors read and approved the final manuscript.

CONFLICTS OF INTEREST

The authors declare no competing interests.

ACKNOWLEDGMENTS

This work is supported by grants from the Natural Science Foundation of China (81872073, 81672511, 81872503, and 81573010); the Liaoning Science and Technology Plan Project (2017225020); the Project of Key Laboratory of Neuro-oncology in Liaoning Province (112-2400017005); a special developmental project guided by the central government of Liaoning Province (2017011553-301); and the Outstanding Scientific Fund of Shengjing Hospital (201802).

REFERENCES

1. Zhu, D., Tu, M., Zeng, B., Cai, L., Zheng, W., Su, Z., and Yu, Z. (2017). Up-regulation of miR-497 confers resistance to temozolomide in human glioma cells by targeting mTOR/Bcl-2. Cancer Med. *6*, 452–462.
2. Giammalva, G.R., Iacopino, D.G., Azzarello, G., Gaggiotti, C., Graziano, F., Gulì, C., Pino, M.A., and Maugeri, R. (2018). End-of-Life Care in High-Grade Glioma Patients. The Palliative and Supportive Perspective. Brain Sci. *8*.
3. Delgado-Bellido, D., Fernández-Cortés, M., Rodríguez, M.I., Serrano-Sáenz, S., Carracedo, A., Garcia-Diaz, A., and Oliver, F.J. (2019). VE-cadherin promotes vasculogenic mimicry by modulating kaiso-dependent gene expression. Cell Death Differ. *26*, 348–361.
4. Xu, Y., Li, Q., Li, X.Y., Yang, Q.Y., Xu, W.W., and Liu, G.L. (2012). Short-term anti-vascular endothelial growth factor treatment elicits vasculogenic mimicry formation of tumors to accelerate metastasis. J. Exp. Clin. Cancer Res. *31*, 16.
5. Nghiemphu, P.L., Ebiana, V.A., Wen, P., Gilbert, M., Abrey, L.E., Lieberman, F., DeAngelis, L.M., Robins, H.I., Yung, W.K.A., Chang, S., et al. (2018). Phase I study of sorafenib and tipifarnib for recurrent glioblastoma: NABTC 05-02. J. Neurooncol. *136*, 79–86.
6. Cai, H.P., Wang, J., Xi, S.Y., Ni, X.R., Chen, Y.S., Yu, Y.J., Cen, Z.W., Yu, Z.H., Chen, F.R., Guo, C.C., et al. (2019). Tenascin-cmediated vasculogenic mimicry formation via regulation of MMP2/MMP9 in glioma. Cell Death Dis. *10*, 879.
7. Angara, K., Borin, T.F., and Arbab, A.S. (2017). Vascular Mimicry: A Novel Neovascularization Mechanism Driving Anti-Angiogenic Therapy (AAT) Resistance in Glioblastoma. Transl. Oncol. *10*, 650–660.
8. Sun, H., Zhang, D., Yao, Z., Lin, X., Liu, J., Gu, Q., Dong, X., Liu, F., Wang, Y., Yao, N., et al. (2017). Anti-angiogenic treatment promotes triple-negative breast cancer invasion via vasculogenic mimicry. Cancer Biol. Ther. *18*, 205–213.
9. Maniotis, A.J., Folberg, R., Hess, A., Seftor, E.A., Gardner, L.M., Pe'er, J., Trent, J.M., Meltzer, P.S., and Hendrix, M.J. (1999). Vascular channel formation by human melanoma cells in vivo and in vitro: vasculogenic mimicry. Am. J. Pathol. *155*, 739–752.
10. Seftor, R.E., Hess, A.R., Seftor, E.A., Kirschmann, D.A., Hardy, K.M., Margaryan, N.V., and Hendrix, M.J. (2012). Tumor cell vasculogenic mimicry: from controversy to therapeutic promise. Am. J. Pathol. *181*, 1115–1125.
11. Hendrix, M.J., Seftor, R.E., Seftor, E.A., Gruman, L.M., Lee, L.M., Nickoloff, B.J., Miele, L., Sheriff, D.D., and Schatteman, G.C. (2002). Transendothelial function of human metastatic melanoma cells: role of the microenvironment in cell-fate determination. Cancer Res. *62*, 665–668.
12. Zhang, X., Zhang, J., Zhou, H., Fan, G., and Li, Q. (2019). Molecular Mechanisms and Anticancer Therapeutic Strategies in Vasculogenic Mimicry. J. Cancer *10*, 6327–6340.
13. Wilson, T.A., Karajannis, M.A., and Harter, D.H. (2014). Glioblastoma multiforme: State of the art and future therapeutics. Surg. Neurol. Int. *5*, 64.
14. de Lemos, M.L., Markarian, A., Chan, E., Schaff, K., and Walisser, S. (2018). Clinical effectiveness of bevacizumab in patients with recurrent brain tumours: A population-based evaluation. J. Oncol. Pharm. Pract. *24*, 33–36.
15. Guo, J., Cai, H., Liu, X., Zheng, J., Liu, Y., Gong, W., Chen, J., Xi, Z., and Xue, Y. (2018). Long Non-coding RNA LINC00339 Stimulates Glioma Vasculogenic Mimicry Formation by Regulating the miR-539-5p/TWIST1/MMPs Axis. Mol. Ther. Nucleic Acids *10*, 170–186.
16. Coppin, L., Leclerc, J., Vincent, A., Porchet, N., and Pigny, P. (2018). Messenger RNA Life-Cycle in Cancer Cells: Emerging Role of Conventional and Non-Conventional RNA-Binding Proteins? Int. J. Mol. Sci. *19*.
17. Yang, Y.H., Markus, M.A., Mangs, A.H., Raitskin, O., Sperling, R., and Morris, B.J. (2013). ZRANB2 localizes to supraspliceosomes and influences the alternative splicing of multiple genes in the transcriptome. Mol. Biol. Rep. *40*, 5381–5395.
18. Cianci, P., Agosti, M., Modena, P., and Selicorni, A. (2019). De novo Xq21.31-q21.32 duplication in intellectual disability: a new report. Clin. Dysmorphol. *28*, 98–100.
19. Bhattacharjee, R.B., and Bag, J. (2012). Depletion of nuclear poly(A) binding protein PABPN1 produces a compensatory response by cytoplasmic PABP4 and PABP5 in cultured human cells. PLoS ONE *7*, e53036.
20. Blanco, P., Sargent, C.A., Boucher, C.A., Howell, G., Ross, M., and Affara, N.A. (2001). A novel poly(A)-binding protein gene (PABPC5) maps to an X-specific subinterval in the Xq21.3/Yp11.2 homology block of the human sex chromosomes. Genomics *74*, 1–11.
21. Zheng, J., Liu, X., Wang, P., Xue, Y., Ma, J., Qu, C., and Liu, Y. (2016). CRNDE Promotes Malignant Progression of Glioma by Attenuating miR-384/PIWIL4/STAT3 Axis. Mol. Ther. *24*, 1199–1215.
22. Shi, X., Sun, M., Liu, H., Yao, Y., and Song, Y. (2013). Long non-coding RNAs: a new frontier in the study of human diseases. Cancer Lett. *339*, 159–166.
23. Ramos, A.D., Attenello, F.J., and Lim, D.A. (2016). Uncovering the roles of long non-coding RNAs in neural development and glioma progression. Neurosci. Lett. *625*, 70–79.

24. Kimura, K., Wakamatsu, A., Suzuki, Y., Ota, T., Nishikawa, T., Yamashita, R., Yamamoto, J., Sekine, M., Tsuritani, K., Wakaguri, H., et al. (2006). Diversification of transcriptional modulation: large-scale identification and characterization of putative alternative promoters of human genes. Genome Res. *16*, 55–65.

25. Gowravaram, M., Schwarz, J., Khilji, S.K., Urlaub, H., and Chakrabarti, S. (2019). Insights into the assembly and architecture of a Staufen-mediated mRNA decay (SMD)-competent mRNP. Nat. Commun. *10*, 5054.

26. Gong, C., and Maquat, L.E. (2011). lncRNAs transactivate STAU1-mediated mRNA decay by duplexing with 3′ UTRs via Alu elements. Nature *470*, 284–288.

27. Maekawa, S., Imamachi, N., Irie, T., Tani, H., Matsumoto, K., Mizutani, R., Imamura, K., Kakeda, M., Yada, T., Sugano, S., et al. (2015). Analysis of RNA decay factor mediated RNA stability contributions on RNA abundance. BMC Genomics *16*, 154.

28. Guo, S., Jian, L., Tao, K., Chen, C., Yu, H., and Liu, S. (2019). Novel Breast-Specific Long Non-coding RNA LINC00993 Acts as a Tumor Suppressor in Triple-Negative Breast Cancer. Front. Oncol. *9*, 1325.

29. Yu, J., Liang, Q.Y., Wang, J., Cheng, Y., Wang, S., Poon, T.C., Go, M.Y., Tao, Q., Chang, Z., and Sung, J.J. (2013). Zinc-finger protein 331, a novel putative tumor suppressor, suppresses growth and invasiveness of gastric cancer. Oncogene *32*, 307–317.

30. Vedeld, H.M., Nesbakken, A., Lothe, R.A., and Lind, G.E. (2018). Re-assessing *ZNF331* as a DNA methylation biomarker for colorectal cancer. Clin. Epigenetics *10*, 70.

31. Wang, S.H., Liou, G.G., Liu, S.H., Chang, J.S., Hsiao, J.R., Yen, Y.C., Chen, Y.L., Wu, W.L., Chang, J.Y., and Chen, Y.W. (2019). Laminin γ2-enriched extracellular vesicles of oral squamous cell carcinoma cells enhance in vitro lymphangiogenesis via integrin α3-dependent uptake by lymphatic endothelial cells. Int. J. Cancer *144*, 2795–2810.

32. Korbakis, D., Dimitromanolakis, A., Prassas, I., Davis, G.J., Barber, E., Reckamp, K.L., Blasutig, I., and Diamandis, E.P. (2015). Serum LAMC2 enhances the prognostic value of a multi-parametric panel in non-small cell lung cancer. Br. J. Cancer *113*, 484–491.

33. Ling, G., Wang, S., Song, Z., Sun, X., Liu, Y., Jiang, X., Cai, Y., Du, M., and Ke, Y. (2011). Transforming growth factor-β is required for vasculogenic mimicry formation in glioma cell line U251MG. Cancer Biol. Ther. *12*, 978–988.

34. Liu, X., Wang, J.H., Li, S., Li, L.L., Huang, M., Zhang, Y.H., Liu, Y., Yang, Y.T., Ding, R., and Ke, Y.Q. (2015). Histone deacetylase 3 expression correlates with vasculogenic mimicry through the phosphoinositide3-kinase / ERK-MMP-laminin5γ2 signaling pathway. Cancer Sci. *106*, 857–866.

35. Brown, E. (2001). Integrin-associated protein (CD47): an unusual activator of G protein signaling. J. Clin. Invest. *107*, 1499–1500.

36. Shinohara, M., Ohyama, N., Murata, Y., Okazawa, H., Ohnishi, H., Ishikawa, O., and Matozaki, T. (2006). CD47 regulation of epithelial cell spreading and migration, and its signal transduction. Cancer Sci. *97*, 889–895.

37. He, Z., Ruan, X., Liu, X., Zheng, J., Liu, Y., Liu, L., et al. (2019). FUS/circ_002136/miR-138-5p/SOX13 feedback loop regulates angiogenesis in Glioma. J. Exp. Clin. Cancer Res. *38*, 65.

38. Batista, P.J., and Chang, H.Y. (2013). Long noncoding RNAs: cellular address codes in development and disease. Cell *152*, 1298–1307.

39. Yang, Y., Chen, L., Gu, J., Zhang, H., Yuan, J., Lian, Q., Lv, G., Wang, S., Wu, Y., Yang, Y.T., et al. (2017). Recurrently deregulated lncRNAs in hepatocellular carcinoma. Nat. Commun. *8*, 14421.

40. McCleland, M.L., Mesh, K., Lorenzana, E., Chopra, V.S., Segal, E., Watanabe, C., Haley, B., Mayba, O., Yaylaoglu, M., Gnad, F., and Firestein, R. (2016). CCAT1 is an enhancer-templated RNA that predicts BET sensitivity in colorectal cancer. J. Clin. Invest. *126*, 639–652.

41. Gao, Y., Yu, H., Liu, Y., Liu, X., Zheng, J., Ma, J., Gong, W., Chen, J., Zhao, L., Tian, Y., and Xue, Y. (2018). Long Non-Coding RNA HOXA-AS2 Regulates Malignant Glioma Behaviors and Vasculogenic Mimicry Formation via the MiR-373/EGFR Axis. Cell. Physiol. Biochem. *45*, 131–147.

42. Wu, W., Yu, T., Wu, Y., Tian, W., Zhang, J., and Wang, Y. (2019). The miR155HG/miR-185/ANXA2 loop contributes to glioblastoma growth and progression. J. Exp. Clin. Cancer Res. *38*, 133.

43. Wang, D., Zheng, J., Liu, X., Xue, Y., Liu, L., Ma, J., He, Q., Li, Z., Cai, H., and Liu, Y. (2019). Knockdown of USF1 Inhibits the Vasculogenic Mimicry of Glioma Cells via Stimulating SNHG16/miR-212-3p and linc00667/miR-429 Axis. Mol. Ther. Nucleic Acids *14*, 465–482.

44. Qi, P., and Du, X. (2013). The long non-coding RNAs, a new cancer diagnostic and therapeutic gold mine. Mod. Pathol. *26*, 155–165.

45. Ji, L., Li, X., Zhou, Z., Zheng, Z., Jin, L., and Jiang, F. (2020). LINC01413/hnRNP-K/ZEB1 Axis Accelerates Cell Proliferation and EMT in Colorectal Cancer via Inducing YAP1/TAZ1 Translocation. Mol. Ther. Nucleic Acids *19*, 546–561.

46. Xu, C.Z., Jiang, C., Wu, Q., Liu, L., Yan, X., and Shi, R. (2016). A Feed-Forward Regulatory Loop between HuR and the Long Noncoding RNA HOTAIR Promotes Head and Neck Squamous Cell Carcinoma Progression and Metastasis. Cell. Physiol. Biochem. *40*, 1039–1051.

47. Jiang, S., Linghu, E., Zhan, Q., Han, W., and Guo, M. (2015). Methylation of ZNF331 Promotes Cell Invasion and Migration in Human Esophageal Cancer. Curr. Protein Pept. Sci. *16*, 322–328.

48. Meiboom, M., Murua Escobar, H., Pentimalli, F., Fusco, A., Belge, G., and Bullerdiek, J. (2003). A 3.4-kbp transcript of ZNF331 is solely expressed in follicular thyroid adenomas. Cytogenet. Genome Res. *101*, 113–117.

49. Wang, Y., He, T., Herman, J.G., Linghu, E., Yang, Y., Fuks, F., Zhou, F., Song, L., and Guo, M. (2017). Methylation of ZNF331 is an independent prognostic marker of colorectal cancer and promotes colorectal cancer growth. Clin. Epigenetics *9*, 115.

50. Park, E., Gleghorn, M.L., and Maquat, L.E. (2013). Staufen2 functions in Staufen1-mediated mRNA decay by binding to itself and its paralog and promoting UPF1 helicase but not ATPase activity. Proc. Natl. Acad. Sci. USA *110*, 405–412.

51. Gong, C., Tang, Y., and Maquat, L.E. (2013). mRNA-mRNA duplexes that autoelicit Staufen1-mediated mRNA decay. Nat. Struct. Mol. Biol. *20*, 1214–1220.

52. Gong, C., Kim, Y.K., Woeller, C.F., Tang, Y., and Maquat, L.E. (2009). SMD and NMD are competitive pathways that contribute to myogenesis: effects on PAX3 and myogenin mRNAs. Genes Dev. *23*, 54–66.

53. Cho, H., Kim, K.M., Han, S., Choe, J., Park, S.G., Choi, S.S., and Kim, Y.K. (2012). Staufen1-mediated mRNA decay functions in adipogenesis. Mol. Cell *46*, 495–506.

54. Kretz, M., Siprashvili, Z., Chu, C., Webster, D.E., Zehnder, A., Qu, K., Lee, C.S., Flockhart, R.J., Groff, A.F., Chow, J., et al. (2013). Control of somatic tissue differentiation by the long non-coding RNA TINCR. Nature *493*, 231–235.

55. Wang, J., Gong, C., and Maquat, L.E. (2013). Control of myogenesis by rodent SINE-containing lncRNAs. Genes Dev. *27*, 793–804.

56. Xu, T.P., Liu, X.X., Xia, R., Yin, L., Kong, R., Chen, W.M., Huang, M.D., and Shu, Y.Q. (2015). SP1-induced upregulation of the long noncoding RNA TINCR regulates cell proliferation and apoptosis by affecting KLF2 mRNA stability in gastric cancer. Oncogene *34*, 5648–5661.

57. Ramos, A., Grünert, S., Adams, J., Micklem, D.R., Proctor, M.R., Freund, S., Bycroft, M., St Johnston, D., and Varani, G. (2000). RNA recognition by a Staufen double-stranded RNA-binding domain. EMBO J. *19*, 997–1009.

58. Damas, N.D., Marcatti, M., Côme, C., Christensen, L.L., Nielsen, M.M., Baumgartner, R., Gylling, H.M., Maglieri, G., Rundsten, C.F., Seemann, S.E., et al. (2016). SNHG5 promotes colorectal cancer cell survival by counteracting STAU1-mediated mRNA destabilization. Nat. Commun. *7*, 13875.

59. Yeo, C., Lee, H.J., and Lee, E.O. (2019). Serum promotes vasculogenic mimicry through the EphA2/VE-cadherin/AKT pathway in PC-3 human prostate cancer cells. Life Sci. *221*, 267–273.

60. Drake, J.M., Barnes, J.M., Madsen, J.M., Domann, F.E., Stipp, C.S., and Henry, M.D. (2010). ZEB1 coordinately regulates laminin-332 and beta4 integrin expression altering the invasive phenotype of prostate cancer cells. J. Biol. Chem. *285*, 33940–33948.

61. El Hallani, S., Boisselier, B., Peglion, F., Rousseau, A., Colin, C., Idbaih, A., Marie, Y., Mokhtari, K., Thomas, J.L., Eichmann, A., et al. (2010). A new alternative mechanism in glioblastoma vascularization: tubular vasculogenic mimicry. Brain *133*, 973–982.

62. Wu, N., Zhao, X., Liu, M., Liu, H., Yao, W., Zhang, Y., Cao, S., and Lin, X. (2011). Role of microRNA-26b in glioma development and its mediated regulation on EphA2. PLoS ONE *6*, e16264.

63. Li, X., Xue, Y., Liu, X., Zheng, J., Shen, S., Yang, C., Chen, J., Li, Z., Liu, L., Ma, J., et al. (2019). ZRANB2/SNHG20/FOXK1 Axis regulates Vasculogenic mimicry formation in glioma. J. Exp. Clin. Cancer Res. *38*, 68.

OMTO, Volume *17*

Supplemental Information

The PABPC5/HCG15/ZNF331 Feedback Loop Regulates Vasculogenic Mimicry of Glioma via STAU1-Mediated mRNA Decay

Fangkun Jing, Xuelei Ruan, Xiaobai Liu, Chunqing Yang, Di Wang, Jian Zheng, Yixue Xue, Shuyuan Shen, Lianqi Shao, Yang Yang, Ping Wang, Jun Ma, and Yunhui Liu

Supplementary tables

Table S1: Primer list of PCR

Gene name	Forward	Reverse
GAPDH	GGAAGCTTGTCATCAATGGAAATC	TGATGACCCTTTTGGCTCCC
PABPC5	CAGATTCAAATTCCCAGAAGAGC	TTTCTTCTGTGCTCGCCCTAC
HCG15	GTGTTAGCCAGGATGGTCTCGATC	CGGTAGCTCACGCCTGTAATCTC
ZNF331	TTCGCCGACGTAGCCATAGAC	CCAGTTACGGCCAAGGGATTTA

Table S2: Sequence of the applied plasmid

Gene name	Sequence
HCG15-RNAi	GAGCTCTATGCCATCCTGCTT
PABPC5-RNAi	AAGTCGTATGCGATGACAA
ZNF331-RNAi	AAACCATCTCCGAGAACAT
STAU1-RNAi	CAGGGCCGCAGGGAGTTTGTGATGCTTCAAGAGAGCATCACAAACTCCCTGCGGCTTTTTG
UPF1-RNAi	CACCGCGAGAAGGACTTCATCATCCTTCAAGAGACGATAACTCCTGAAATCCAGCTTTTTG

HCG15(+), ZNF331(+), STAU1(+) were full-length gene sequence.

Gene name	non-targeting sequences
HCG15-RNAi	GATCCCGAGCTCTATGCCATCCTGCTTCTCGAGAAGCAGGATGGCATAGAGCTCTTTTTGGAT
PABPC5-RNAi	GATCCAAAAAGAGCAACTTTCACCAATGTTTCTCGAGAAACATTGGTGAAAGTTGCTC
ZNF331-RNAi	GATCCCctAAACCATCTCCGAGAACATCTCGAGATGTTCTCGGAGATGGTTTAG TTTTTGGAT
STAU1-RNAi	CAGGGCCGCAGGGAGTTTGTGATGCTTCAAGAGAGCATCACAAACTCCCTGCGGCTTTTTG
UPF1-RNAi	CACCGCGAGAAGGACTTCATCATCCTTCAAGAGACGATAACTCCTGAAATCCAGCTTTTTG

Table S3: Primer sequence of ChIP

Gene name	Forward	Reverse	Product size
Control	AGAAACTAAGGATCACAGAAAGCAA	TCTAGTGGCCAAAAGTTGAGG	100bp
LAMC2	TCTGCACTAAAATGAAATCTTCC	ATTTTCCCTTCTAGTCGCTGGT	150bp
Gene name	Forward	Reverse	Product size
Control	TGTGACTACTATCCAGTAGAACTTGG	TCCATATGAAGCAGCAATCCT	166bp
PABPC5	TGCCATTGGGCTTTTGATAG	GCAATTAGGCCAGAGAAGGA	177bp

Supplementary Figure

Figure S1

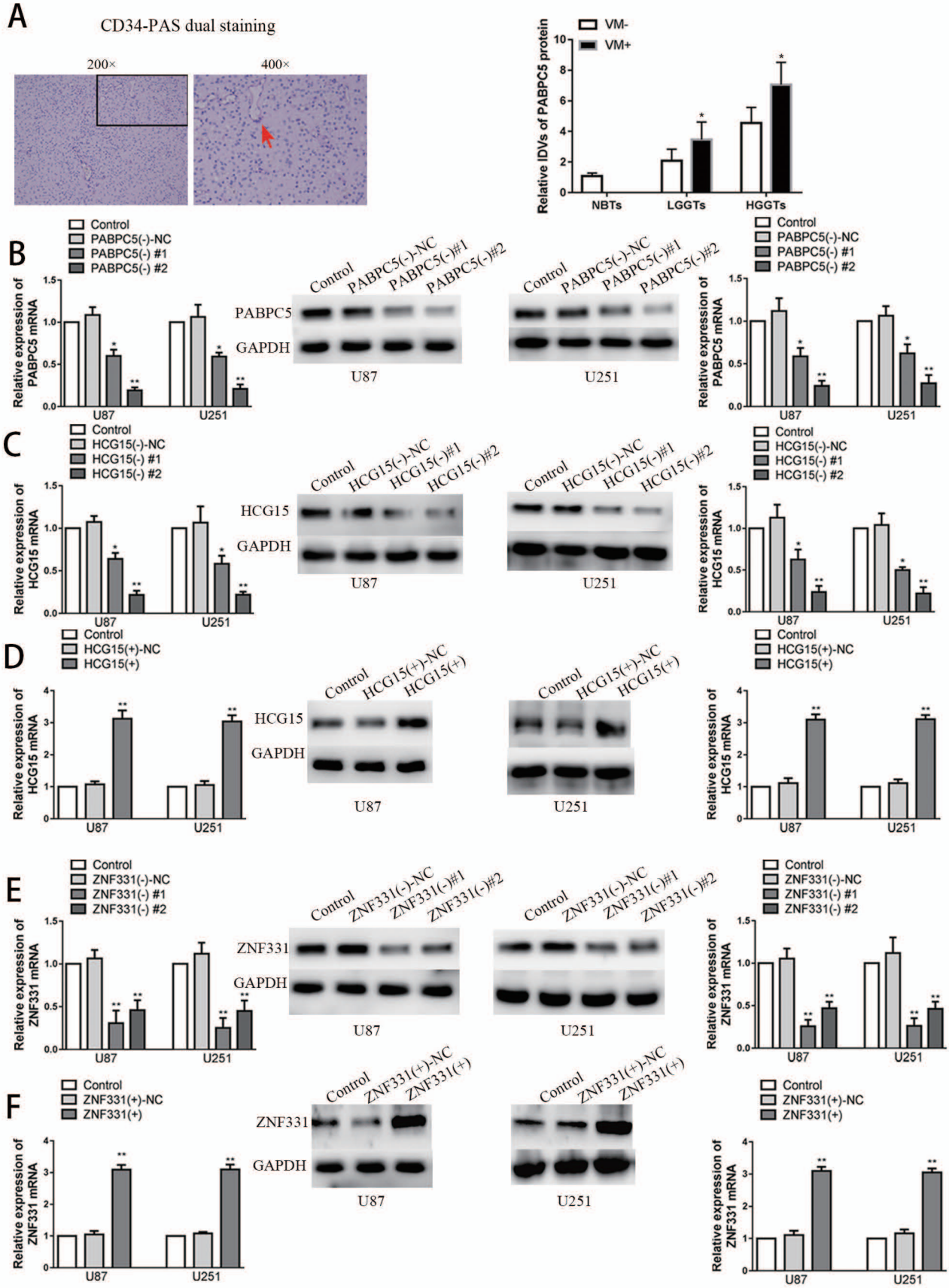

Supplementary Legend

(A) Typical CD34-PAS dual staining of VM and correlation between *PABPC5* and VM. (B) The Expressional efficiency of knockdown of *PABPC5* in U87 and U251 cells. Data are presented as mean ± SD (n=3). ***P*< 0.01, **P*<0.05 *vs. PABPC5(-)-NC* group. (C) The Expressional efficiency of knockdown of *HCG15* in U87 and U251 cells. Data are presented as mean ± SD (n=3). ***P*<0.01, **P*<0.05 *vs. HCG15(-)-NC* group. (D) The Expressional efficiency of overexpression of *HCG15* in U87 and U251 cells. Data are presented as mean ± SD (n=3). ***P*<0.01, **P*<0.05 *vs. HCG15(+)-NC* group. (E) The Expressional efficiency of knockdown of *ZNF331* in U87 and U251 cells. Data are presented as mean ± SD (n=3). ***P*<0.01, **P*<0.05 *vs. ZNF331(-)-NC* group. (F) The Expressional efficiency of overexpression of *ZNF331* in U87 and U251 cells. Data are presented as mean ± SD (n=3). ***P*<0.01, **P*<0.05 *vs. ZNF331(+)-NC* group.